WIP transcriptional regulators modulate developmental progression in both life cycle phases of a moss

Maria Victoria Gomez Roldan[1†], Yuhang Yan[1], Yujuan Du[1], Florence Charlot[2], Pierre-François Perroud[2], Julie Calbry[2], Ofir Griess[3], Marion Verdenaud[1], Fabien Marcel[1], Sylvie Citerne[2], Joseph Tran[1], Nir Ohad[3], Yoan Coudert[4], Fabien Nogué[2], Abdelhafid Bendahmane[1†]

[1]Université Paris-Saclay, CNRS, INRAE, Université d'Evry, Institute of Plant Sciences Paris-Saclay (IPS2), 91405, Orsay, France

[2]Université Paris-Saclay, INRAE, AgroParisTech, Institute Jean-Pierre Bourgin for Plant Science (IJPB), 78000, Versailles, France.

[3]School of Plant Sciences and Food Security, Tel-Aviv University, 69978, Tel- Aviv, Israel.

[4]Laboratoire Reproduction et Développement des Plantes, Université de Lyon, ENS de Lyon, UCB Lyon 1, CNRS, INRAE, INRIA, Lyon 69007, France

[†] Corresponding authors: Maria Victoria Gomez Roldan, Abdelhafid Bendahmane,

Email: victoria.gomez@cnrs.fr; abdelhafid.bendahmane@inrae.fr,

Author Contributions: MVGR and AB conceived the study. MVGR, YY, YD, YC and OG designed and performed the plant experiments. FC, PFP, JC and FN generated the transgenic *P. patens* lines. JT, MV, and MVGR analyzed RNA-seq and DAP-seq data. SC performed auxin quantification. FM helps with sequencing facilities. FN, YC and NO helped with the interpretation of the data. MVGR and AB wrote the paper with contributions from all authors.

Competing Interest Statement: The authors declare no competing interests.

Classification: Biological Sciences; Developmental Biology; Evolution; Plant Biology.

Keywords: *Physcomitrium patens*, WIP transcription factors, polysety, protonema, auxin

This PDF file includes:

Main Text
Figures 1 to 4

Abstract (198 words)

The sexual life cycle of bryophytes and vascular plants, the two extant lineages of land plants, is dominated by a gametophytic and a sporophytic phase, respectively. Body plan diversification in these two phases has followed separate evolutionary trajectories in both lineages. However, how evolutionary conserved gene families have accompanied body plan diversification remains poorly understood. WIP transcription factors are conserved in land plants, and their function has been associated with root and flower development in angiosperms. Here, we dissect the function of Pp*WIP1 and PpWIP2* genes in a model bryophyte, the moss *Physcomitrium patens*. We demonstrate that Pp*WIP*s are expressed during both phases of the life cycle and regulate specific developmental processes. In the gametophytic phase, Pp*WIP*s promote the chloronema-to-caulonema transition, but restrict gametophore development. In the sporophytic phase, Pp*WIPs* prevent polysety, the formation of multiple sporogonia. RNA-seq, DAP-seq and hormone analysis revealed that both *P. patens* and *A. thaliana* proteins act by controlling auxin homeostasis. Inter-species complementation experiments revealed that Pp*WIP*s are partially able to substitute At*WIP* molecular function in Arabidopsis root and seeds. Our findings demonstrate that WIPs control developmental progression in both phases of the land plant life cycle through an evolutionarily conserved molecular function.

Significance Statement - 115

The sporophytic and gametophytic phases of land plants, which together constitute the sexual life cycle, exhibit distinct body plans that have taken separate evolutionary paths. Here, we investigate the evolution of *WIP* gene functions in the control of these divergent body plans using *Physcomitrium patens* and *Arabidopsis thaliana*. We show that, in the gametophyte of *P. patens*, PpWIPs regulate the chloronema-to-caulonema transition and repress polysety, likely through the direct regulation of auxin biosynthesis genes. These findings indicate a partial conservation of the WIP gene regulatory network during land plant evolution.

Introduction

From aquatic to terrestrial habitats, the success of land plants is achieved through a multitude of evolutionary innovations, such as gas-exchanging structures, vascular tissues, rooting systems, reproductive organs and an alternation of generations. Two morphologically distinct sporophytic and gametophytic phases (generations) constitute the sexual life cycle of extant land plants (1). In bryophytes, haploid gametophytes dominate and nourish diploid sporophytes (2,3). Tracheophytes (vascular plants) exhibit relatively greater levels of specialized vegetative growth in sporophytes and show reductions in the size and complexity of gametophytes (1). The plant body plan of these two life phases has taken separate evolutionary paths and diversified to adapt to *terra firma*. The understanding of how conserved gene families have accompanied the diversification of plant body plans is however still sketchy.

Gene duplication is often considered as one of the key drivers of evolutionary innovation. Duplicate genes can acquire novel functions, providing the genetic basis for adaptive morphological and physiological innovations (4). Our study focuses on the characterization of a subgroup of A1d C2H2 zinc finger WIP transcription factors that exhibits an expansion in gene copy number (5–12). WIP proteins are characterized by a highly conserved C-terminal DNA binding domain with three conserved amino acids, tryptophan (W), isoleucine (I), and proline (P). They are involved in the development of distinct plant organs in both sporophytic and gametophytic phases. In bryophytes, there is overall a limited number of *WIP* gene copies. The liverwort *Marchantia polymorpha* carries a single *WIP* gene, *MpWIP*, which is required for the morphogenesis of the air pore complex in the gametophyte (13). In contrast, the moss *P. patens* harbors two *WIP* gene copies, while other moss species harbor from one to multiple *WIP* genes, indicating lineage-specific expansions. In flowering plants, *WIP* genes are multi-copies and their functions are diverse. In *Arabidopsis thaliana*, *AtWIP1/TRANSPARENT TESTA1* (*AtWIP1*) is involved in seed coat development and mutations in *AtWIP6* (*dot5*) results in leaf vein pattern defects (9,14). *AtWIP2*/*NO-TRANSMITTING-TRACT* (*NTT*) and two closely related paralogues (*AtWIP4* and *AtWIP5*) are redundantly required for the initiation of the primary root meristem. Roots are absent in *nww Arabidopsis* mutant plants lacking all three genes (*NTT*, *WIP4* and *WIP5*) (8), and cross-communication between spatially expressed *WIPs* drives embryonic root development (11). Moreover, transmitting tract development in single *wip2*/*ntt* mutants is defective, which inhibits pollen tubes to grow further in the carpel, causing a reduced number of fertilized ovules in the basal part of the silique (7). Likewise, our previous work has shown that in the angiosperm *Cucumis melo*, *CmWIP1* inhibits carpel development, leading to the production of male unisexual flowers (15).

Despite the fact that the gametophytic body of bryophytes and the sporophytic body of tracheophytes have evolved separately, different investigations have shown that similar genetic toolkits were co-opted to regulate the development of analogous organs (16–21). The moss *Physcomitrium patens* uniquely combines ancestral features (e.g. adaptation to water loss and growth against gravity) while also exhibiting derived morphological traits (e.g. leaf-like organs) (22), serving as a compelling model to study the homology and evolution of key phenotypic novelties of land plants (18). Here, we investigate the evolutionary conservation of *WIP* gene function in *Physcomitrium patens* revealing central role in vegetative and reproductive development.

Results

Molecular phylogeny of WIP Proteins

From the *P. patens* genome, two genes were identified *Pp3c15_17790* and *Pp3c9_22230,* coding for two proteins named here PpWIP1 and PpWIP2, respectively. We first analyzed their molecular phylogeny by comparing their protein sequences with WIPs curated from several database sources (Phytozome, 1000 Plant Transcripts) (Dataset S1) (23,24). Our analysis separates WIP proteins from bryophytes and vascular plants (Fig. S1). The first clade includes MpWIP from *M. polymorp*ha and PpWIP1 and PpWIP2 from *P. patens*. The second clade can be subdivided in several subgroups, on which the first group (A) includes AtWIP6 from *A. thaliana* and several gymnosperms. The next group (B) includes AtWIP2/NTT, AtWIP4, AtWIP5 and CmWIP1, associated with root and flower development in *Arabidopsis* and melon; as well as GhWIP2, previously shown to be involved in petal cell expansion in *Gerbera hybrida* (25). The third group (C) includes AtWIP1/TT1, AtWIP3 and its homologues (Fig. S1).

Although all WIP proteins share a highly conserved C-terminal zinc finger domain involved in DNA binding, their N-terminal regions are more divergent (10). To examine this variability, we performed a MEME motif analysis on a selected set of WIP proteins and identified three conserved motifs: the WIP signature motif (M1) and two additional motifs (M2 and M3) predicted to mediate protein–protein interactions, consistent with the reported recruitment of TOPLESS/TOPLESS-RELATED (TPL/TPR) proteins by CmWIP1 (26) (Fig. 1A; Fig. S2). Motifs M1 and M2 were conserved across all analyzed WIP proteins, whereas the M3 motif was detected only in AtWIP2/NTT homologues and in both WIP proteins from *P. patens*. This distribution suggests that PpWIPs may share certain molecular functions with group B AtWIPs. By contrast, MpWIP lacks the M3 motif (Fig. 1A), suggesting possible structural divergence within bryophyte WIPs. Nevertheless, the strong conservation of the C-terminal region across land plants, which constitutes most of the WIP protein sequence, suggests that core WIP functions are likely maintained even in proteins lacking the M3 motif (Fig. S3A).

PpWIPs are expressed in Gametophytic and Sporophytic Tissues

To unravel the role of *PpWIPs*, we first examined their expression pattern throughout the moss life cycle. *P. patens* forms eight types of stem cells, seven in the haploid gametophyte and one in the diploid sporophyte (27). The haploid phase includes the development of filamentous cells called protonema and leafy shoots called gametophores. Protonema consists of two types of cells, chloronema and caulonema (2). Immediately after the spore germination, a chloronema apical stem cell is formed to produce chloronema cells. Along with the plant growth, chloronema apical stem cells transform into caulonema apical stem cells that will produce caulonema cells (27,28). Chloronema cells are abundant in chloroplasts and divide perpendicularly to the growth axis, while caulonema cells contain fewer chloroplasts and divide obliquely to the growth axis (29). Tetrahedral apical stem cells are usually specified from caulonema cells, leading to the formation of gametophore bearing at their base filamentous cells with a rooting function called rhizoids (30).

To investigate the spatial and temporal accumulation of PpWIP proteins, we generated translational β-glucuronidase (GUS) reporter lines. The GUS coding sequence was inserted in frame immediately upstream of the endogenous stop codon at the *PpWIP1* and *PpWIP2* loci by homologous recombination (Fig. S4A). Correct integration of the GUS cassette was verified by PCR amplification across the 5′ and 3′ recombination junctions and by genome-wide Illumina sequencing of the resulting lines, confirming precise in-frame insertion and the absence of additional genomic insertions (Fig. S4A–B; Fig. S5A). GUS staining of these reporter lines revealed expression of both PpWIP1 and PpWIP2 throughout the gametophytic phase, with detectable signals in protonema tissue, early gametophore buds, and gametophore stems (Fig. 1B).

The GUS reporter lines failed to produce sporophytes. Although the cause of this sterility remains unknown, the WIP–GUS fusion may disrupt normal WIP protein function by altering its three-dimensional structure and generating a dominant-negative form that interferes with the regulation of downstream targets required for sporophyte development. To circumvent this limitation, we assessed the expression of *PpWIP1* and *PpWIP2* during the sporophytic phase by RT–qPCR using the WT line. Transcript levels were analyzed in gametophore apices induced for 15 days at 15 °C, as well as in immature (green) and mature (brown) sporophytes. The sporophyte-specific markers *PpBELL1* and *PpKNOX1* were used to validate sporophytic tissue identity (Fig. S4C) (31). We found both *PpWIP1* and *PpWIP2* expressed across the analyzed sporophytic stages, supporting roles beyond the gametophytic phase. These expression patterns are consistent with publicly available transcriptomic data from the PEATmoss database, which report *PpWIP1* and *PpWIP2* expression in protonema, gametophores, and sporophytes (Fig. S3B–C) (32). Taken together, the translational GUS reporter analyses and PEATmoss transcriptomic profiles reveal that *PpWIP1* and

PpWIP2 are expressed during both the gametophytic and sporophytic phases of the *P. patens* life cycle.

PpWIPs Promote Chloronema-to-Caulonema Transition

To investigate the function of *PpWIPs* in *P. patens*, we generated loss-of-function mutants for *PpWIP1* and *PpWIP2* by homologous recombination (hereafter *wip1* and *wip2*; Fig. S6A). Double mutants (*wip1wip2*) were obtained by inter-crossing single mutants, and genotypes were validated by PCR and Illumina sequencing (Fig. S5B; Fig. S6B). As expected, *PpWIP1* and *PpWIP2* transcripts were not detected in the double mutants (Fig. S6C). We compared protonemal development of wild type (WT), single mutants, and *wip1wip2* germinated spores on BCD medium, which promotes caulonema formation. Unlike WT and single mutants, *wip1wip2* plants displayed a compact morphology with shorter cells, indicating functional redundancy between PpWIP1 and PpWIP2 (Fig. 2A–D; Fig. S7A–C). After 16 days, elongated caulonema filaments characteristic of WT were largely absent in the double mutant (Fig. S8A). To further investigate the role of *PpWIPs* in caulonema filament development, we cultured the protonema under unilateral red light, which induces the transition from chloronema to caulonema (Fig. S8*B*) (33). The filaments in the *wip1wip2* double mutant were predominantly composed of highly branched green chloronema cells (Fig. S8*B*). This finding underscores the role of *PpWIPs* in the transition from chloronema to caulonema stem cells during the early stages of moss development. Since gametophores arise from caulonema, we next examined gametophore development in the mutants. After three weeks on BCD+AT medium, *wip1wip2* double mutants produced gametophores comparable to WT and single mutants, indicating that *PpWIPs* are dispensable for gametophore specification (Fig. 2E–F; Fig. S7B–E). However, prolonged growth on BCD medium (2 months) revealed a marked reduction in the formation of new peripheral gametophores in *wip1wip2* plants, consistent with compromised caulonema development (Fig. 2G–H; Fig. S7F–G). Moreover, gametophores in the double mutant were significantly more elongated than those of WT and single mutants, revealing a redundant role for *PpWIPs* in restraining gametophore growth (Fig. 2I–J; Fig. S7D–E). These defects in caulonema development and gametophore growth were consistently observed in independent CRISPR-generated *wip1*Δ and *wip2*Δ single and *wip1*Δ*wip2*Δ double mutants lacking the entire coding sequences of the genes (Fig. S9; Fig. S10). Together, these findings show that *PpWIPs* are not required for gametophore specification but instead act redundantly to promote caulonema differentiation and limit gametophore elongation.

PpWIPs Repress Polysety in *P. patens*

In response to environmental stimuli, egg- and sperm-producing organs (archegonia and antheridia) form at the gametophore apex. Fertilization occurs when a sperm cell enters the archegonium and fuses with the egg, marking the transition to the diploid sporophytic phase of the life cycle (27). Subsequent development of the zygote gives rise to a uniaxial structure, termed the sporogonium (but often referred to as the sporophyte). In *P. patens*, a single sporogonium typically develops per gametophore apex, a condition known as monosety (34). In contrast to monosety, some bryophytes exhibit polysety, in which multiple sporogonia arise from independently fertilized archegonia at a single apex; however, the genetic determinants of this trait are unknown (34–36).

Whereas WT gametophores were predominantly monosetous, *wip1wip2* mutants frequently exhibited polysety, with two to four sporogonia developing at a single apex (Fig. 2K, L). Polysetous gametophores accounted for 4.8% of the *wip1wip2* population, compared with 0.7% in WT. These sporogonia were spatially distinct and displayed heterogeneous pigmentation, ranging from light green to dark brown, indicative of asynchronous development and suggesting independent fertilization events (Fig. 2L). Analysis of single mutants revealed that *wip1* lines showed an increased frequency of gametophores bearing a single sporogonium (40% versus <20% in WT), together with a low but significant incidence of polysety (2.4%) (Fig. S7H). In contrast, *wip2* mutants exhibited markedly reduced sporulation (Fig. S7H). To independently validate these findings, we phenotyped CRISPR–Cas9-edited lines carrying complete deletions of *PpWIP1* and *PpWIP2* (from ATG to stop; Fig. S9A–C). Like for the protonema and the gametophore phenotyping, the CRISPR-generated *wip1*Δ*wip2*Δ double mutants showed a phenotype comparable to that of the recombinant double mutants, with an increased frequency of polysety (Fig. S10A–E). Single edited mutants (*wip1*Δ and *wip2*Δ) showed milder phenotypes and largely resembled WT plants (Fig. S10A-E). Notably, *wip2*Δ mutants exhibited an elevated frequency of single and double sporogonia (6%) compared with WT (<1%) and *wip1*Δ (3%), indicating that repression of polysety in *P. patens* likely involves the combined activity of both PpWIPs.

PpWIPs regulate genes linked to chloronema–caulonema transition.

To elucidate the molecular networks through which *PpWIPs* regulate early gametophyte development in *P. patens*, we compared protonema transcriptomes of WT and *wip* mutants (Fig. S11A–C; Dataset S2). RNA-seq analysis of the *wip1wip2* double mutant identified 2,156 differentially expressed genes (DEGs) relative to WT, including 1,522 down-regulated and 634 up-regulated genes (Fig. 3A). In contrast, single mutants displayed significantly less transcriptional changes, with 1,224 DEGs in *wip1* and 729 DEGs in *wip2*, further supporting functional redundancy between *PpWIP1* and *PpWIP2* (Fig. S11D–H; Dataset S2). Moreover, more than half of the DEGs identified in the *wip1wip2* double mutant (1112 genes) remained unchanged in both the *wip1* and

wip2 single mutants (Fig. S11G), further supporting this functional redundancy. Nevertheless, the larger number of DEGs in *wip1* compared with *wip2* suggests a more prominent contribution of *PpWIP1* to the double-mutant phenotype. Gene Ontology (GO) analysis of down-regulated genes in *wip1wip2* revealed significant enrichment for categories associated with photosynthesis, cell wall organization, and responses to cytokinin and auxin (Fig. 3B; Dataset S3). While, up-regulated genes were enriched for developmental processes, including organ formation, cellular senescence, and responses to ethylene (Fig. 3B; Dataset S3). Only a limited number of GO terms were uniquely enriched in the single mutants (e.g., cell aging in *wip2* and asymmetric division in *wip1*), indicating that while *PpWIPs* share overlapping regulatory roles, each gene may also contribute to distinct transcriptional programs.

Given the defects observed in caulonema formation, we next examined whether transcriptional changes in *wip1wip2* correlated with cell fate transitions during protonema development. We compared our DEG dataset with the published single-cell transcriptomic atlas of *P. patens* that define gene signatures associated with chloronema and caulonema cell identities (37). This analysis revealed that down-regulated genes in *wip1wip2* were preferentially enriched among caulonema cluster genes (cluster 4; 2.6%), whereas up-regulated genes were more strongly associated with chloronema clusters (clusters 0 and 1; 5%) (Fig. S12A; Dataset S4). These findings suggest that impaired activation of caulonema gene expression programs underlies the *wip1wip2* phenotype.

To identify direct transcriptional targets of PpWIPs, we performed DNA affinity purification sequencing (DAP-seq) using the C-terminal DNA-binding domains of PpWIP1 and PpWIP2 (Fig. S13A; Dataset S5) (38,39). Genome-wide binding profiles revealed 3,568 and 1,490 putative target genes for PpWIP1 and PpWIP2, respectively, with binding sites distributed across promoter, intergenic, and gene body regions (Fig. 3C). Notably, both proteins bound the *PpWIP2* locus, spanning promoter and coding regions, pointing to a feedback loop regulation of *PpWIP2* expression (Fig. S13B).

Motif analysis identified a consensus WIP-binding sequence previously characterized in Arabidopsis by ChIP-seq and DAP-seq as highly enriched in the binding sites of both PpWIP1 and PpWIP2 (p = 1e−734 and 1e−270, respectively) (Fig. 3D; Fig. S13C; Fig. S14B; Dataset S6) (12,26,38,39). Integration of DAP-seq and RNA-seq datasets identified 293 genes that were both bound by PpWIPs and differentially expressed in the *wip1wip2* mutant (Fig. 3E; Dataset S7). Among these targets were *P. patens* homologs of *Arabidopsis* genes involved in root hair development (*PpROOT HAIR SPECIFIC 6, PpRHS6*), flowering (*PpFLOWERING BHLH 1, PpFBH1*), and female gametophyte differentiation (*PpAGAMOUS-LIKE61, PpAGL61*) (40,41).

Additional targets included Arabidopsis homologs implicated in shoot branching (*PpCAROTENOID CLEAVAGE DIOXYGENASE 7, PpCCD7*) and cytokinin degradation (*PpCYTOKININ OXIDASE/DEHYDROGENASE 1, PpCKX1*) (42,43), in line with the developmental phenotypes observed in *wip1wip2* double mutants (Fig. S14A; Dataset S7).

PpWIPs Transcriptionally Modulate Auxin Homeostasis

The striking conservation of WIP protein sequences across bryophytes and flowering plants suggests conserved molecular functions. To identify such functions, we compared the predicted target genes of *PpWIPs* with those previously reported for *Arabidopsis* group B WIPs (*AtWIP2/4/5*) (39) (Dataset S8). This analysis revealed a shared enrichment for genes involved in auxin biosynthesis and transport, including members of the *YUCCA* family and *AUXIN TRANSPORT PROTEIN 1* (*AUX1*) (Fig. S14B) (44). Auxin is a central regulator of plant development and has been shown to promote the chloronema-to-caulonema transition in *P. patens* gametophytes (30). Consistent with this, integration of our RNA-seq data from the *wip1wip2* double mutant with previously published RNA-seq datasets from auxin-signaling *P. patens* mutants (45) (Fig. S12B-C), together with DAP-seq analyses, identified *PpYUCC* as a direct target of *PpWIPs*. PpWIP binding was detected within the *PpYUCC* gene body, and *PpYUCC* transcript levels were significantly reduced in *wip1wip2* protonema (Fig. 3F; Fig. S15A–B). Direct binding of *PpWIPs* to *PpYUCC* was confirmed by electrophoretic mobility shift assays (EMSA), which showed a specific shift of a biotin-labeled probe corresponding to the DAP-seq–identified cis-regulatory region; this shift was abolished by competition with unlabeled probe (Fig. 3G). To assess the role of *PpWIPs* in auxin biosynthesis, we quantified endogenous auxin levels in protonema derived from WT and *wip1wip2* spores after 16 days of growth. Indole-3-acetic acid (IAA) levels were significantly reduced in *wip1wip2* protonema compared with WT (Fig. S15C), indicating that *PpWIPs* promote auxin biosynthesis to maintain appropriate auxin levels in protonema tissues. However, supplementation of the growth medium with 5 µM 1-naphthaleneacetic acid (NAA) failed to fully restore the chloronema-to-caulonema transition in the mutant (Fig. S15D), suggesting that *PpWIPs* regulate auxin homeostasis in a context-dependent manner beyond auxin availability alone.

DAP-seq analysis further revealed binding of PpWIPs to a second auxin biosynthesis gene, *PpYUCA*, which is highly expressed in maturing sporophytes (46) (Fig. S15A). This prompted us to ask whether the polysety observed in *wip1wip2* mutants could result from altered endogenous auxin levels. To address this, we analyzed *PpYUCA* expression in gametophore apices harvested 15 days after transfer to 15 °C, and found the gene highly expressed in *wip1* and *wip1wip2* apices relative to WT (Fig. S15E). To test whether elevated auxin levels were sufficient to induce polysety, WT plants were treated with 25 nM 1-naphthaleneacetic acid (NAA) during reproductive organ and

sporogonium development. Auxin-treated plants displayed an increased proportion of fertile apices and, in some cases, multiple sporogonia per apex developed compared with mock-treated controls (Fig. S15F, G). Together, these results indicate that PpWIPs modulate endogenous auxin levels in a phase-specific manner during the *P. patens* life cycle: promoting auxin biosynthesis in protonema to drive the chloronema-to-caulonema transition, while limiting auxin accumulation in gametophore apices to suppress polysety.

Partial functional conservation of WIP proteins across land plants

MEME motif analysis showed that PpWIP proteins are structurally most similar to group B WIP proteins from flowering plants, including AtWIP2/NTT (Fig. 1A). To test whether this similarity reflects conserved molecular function, we performed interspecies complementation assays in *Arabidopsis thaliana*. We generated transgenic lines by guiding expression of Pp*WIPs* in the embryonic root of *nww* mutants and in the transmitting tract of *wip2*/*ntt* mutants by using a 4.1-kb At*WIP4* promoter (*promAtWIP4*) and a 4.6-kb At*WIP2* promoter (*promAtWIP2*), respectively (Fig. 4; Fig. S16*A*). As expected, promoter-driven expression of the corresponding Arabidopsis genes fully rescued the rootless phenotype of *nww* mutants and the absence of the transmitting tract in *wip2/ntt* mutants, validating the experimental system (Fig. 4A–C; Fig. S16B).

Expression of *PpWIP1* or *PpWIP2* under the *promAtWIP4*, rescued root formation in *nww* mutants (Fig. 4*C*), although the resulting primary roots were shorter, agravitropic, and contained fewer or no amyloplast-containing columella cells, indicating ongoing defects in distal root differentiation (Fig. 4*D-F*). In contrast, expression of *PpWIP1* or *PpWIP2* driven by the *AtWIP2* promoter failed to rescue transmitting tract development in *wip2/ntt* mutants (Fig. S16C). Although auxin-related genes are conserved targets in both *P. patens* and Arabidopsis (Fig. S14*B*), these complementation experiments suggest that the molecular functions of PpWIPs and Group B AtWIPs are only partially conserved over evolutionary time.

To further assess evolutionary conservation with other WIP classes, we expressed *PpWIP1* and *PpWIP2* in the seed coat of transparent testa (*wip1/tt1-3*) mutants under the control of the *AtWIP1/TT1* promoter (2 kb). Analysis of proanthocyanidin accumulation in immature seeds and cyanidin levels in mature seeds revealed a clear, but incomplete rescue of the transparent testa phenotype (Fig. S17B–C). This partial complementation suggests limited functional conservation between PpWIPs and group C AtWIPs, which lack the M3 motif.

Together, these experiments suggest that, although Physcomitrium WIP proteins share similar biochemical features with Arabidopsis WIPs, likely reflecting an ancestral property of land plants, functional divergence has occurred following the separation of bryophyte and angiosperm lineages.

Discussion

The diversification of land plant body plans involved distinct innovations in the gametophytic and sporophytic generations. Although these two phases followed different evolutionary trajectories in bryophytes and vascular plants, growing evidence from gene expression patterns indicates that conserved regulatory modules are active in both generations and have been repeatedly deployed to control analogous developmental processes in bryophytes and ferns (17,18,47–50). Our findings identify WIP transcription factors as one such module and demonstrate that *PpWIP1* and *PpWIP2* contribute to developmental regulation across both phases of the *Physcomitrium patens* life cycle.

In the gametophytic phase, PpWIPs act redundantly to promote the transition from chloronema to caulonema, a developmental step required for filament elongation and plant expansion. Loss of both genes prevents the establishment of caulonema identity, resulting in compact protonema tissue enriched in chloronema cells. Transcriptomic analyses, together with comparisons to single-cell expression datasets, support this interpretation, as genes down-regulated in the *wip1wip2* mutant are preferentially associated with caulonema cell fate. These results place PpWIPs upstream of transcriptional programs that control protonema stem cell transitions.

Our combined RNA-seq, DAP-seq, EMSA, and hormone quantification analyses indicate that PpWIPs regulate auxin biosynthesis by directly targeting *YUCCA* genes. In protonema, PpWIPs activate the expression of *PpYUCC*, thereby maintaining endogenous auxin levels required for caulonema differentiation. Consistent with this model, *PpYUCC* is also differentially expressed in *aux/iaaD* mutants, which, like *wip1wip2*, display severe defects in caulonema formation (45), suggesting a shared impairment in auxin signaling responses. Recent studies in the liverwort *Marchantia polymorpha* have demonstrated that the initiation of *de novo* meristems requires a localized apical auxin signaling minimum (51,52). Given that *PpWIP* genes appear to impact the transcriptional landscape of auxin-related genes, it is therefore possible that PpWIP1 and PpWIP2 are required to modulate auxin distribution or sensitivity; in their absence, the inability to establish a precise auxin minimum may inhibit the specification of new apical cells, leading to the observed reduction in the formation of new peripheral gametophores in the *wip1wip2* double mutants.

Beyond their role in gametophytic development, our results implicate PpWIPs in sporophytic patterning through repression of polysety. Whereas wild-type *P. patens* typically forms a single sporogonium per gametophore apex, *wip1wip2* mutants frequently develop multiple sporogonia. Whether this polysety repression relies on an autonomous role of PpWIPs within unfertilized archegonia or on a non-autonomous signal originating from the developing sporophyte remains unresolved. However, the asynchronous development and heterogeneous pigmentation of sporogonia formed on the same gametophore apex suggest that individual archegonia retain

fertilization competence independently, consistent with a local repression mechanism acting at the level of the archegonia. We further found that polysety is associated with elevated *PpYUCA* expression in reproductive tissues and can be recapitulated by auxin treatment of wild-type plants. These observations link auxin accumulation to increased reproductive output and suggest that PpWIPs restrict auxin levels in gametophore apices to limit the number of fertilization events or developing sporogonia. Notably, after fertilization of a single archegonium, neighboring archegonia normally lose fertilization competence, a process involving auxin-regulated terminal differentiation and cell death of canal cells in mosses (53). Disruption of WIP-mediated auxin homeostasis may therefore impair this regulatory mechanism, providing a potential molecular explanation for the emergence of polysety.

Several studies highlight that auxin-mediated control of stem cell behavior is a conserved and central feature of land plant development, illustrating how local auxin biosynthesis, transport, and feedback regulation coordinate stem cell maintenance and differentiation across diverse developmental contexts (17,30,54–56). In melon, CmWIP1 modulates auxin-responsive gene expression through interaction with the transcriptional corepressors *TOPLESS/TOPLESS-RELATED* via a conserved EAR motif (Ethylene-responsive element binding factor–Associated Repression motif) located in the internal region of WIP proteins (26). More broadly, variation in the presence or absence of conserved motifs within the N-terminal regions of WIP proteins, together with differences in the availability or expression of interacting cofactors, likely accounts for the contrasting effects of WIPs on *YUCCA* gene expression, and auxin homeostasis in general. This diversification of WIP-mediated protein–protein interactions provides a plausible explanation for the partial functional conservation observed in interspecies complementation assays: although *PpWIPs* can restore root initiation in *nww* mutants, they fail to rescue transmitting tract formation in *wip2/ntt* mutants and only partially complement the transparent testa phenotype. Collectively, these findings suggest that WIP proteins retain core regulatory functions while undergoing lineage-specific specialization associated with the evolution of novel developmental contexts in flowering plants.

Together, our results identify *PpWIPs* as central regulators of developmental transitions in both the gametophytic and sporophytic phases of *P. patens*, acting in part through the regulation of auxin homeostasis. Several studies highlight that auxin-mediated control of stem cell behavior is a conserved and central feature of land plant development, illustrating how local auxin biosynthesis, transport, and feedback regulation coordinate stem cell maintenance and differentiation across diverse developmental contexts (56). Transcriptomic analyses further indicate that *PpWIP1* and *PpWIP2* function in a partially redundant manner, with additive effects in the double mutant and

distinct regulatory contributions in single mutants, highlighting how an evolutionarily conserved transcription factor family has been redeployed to control life-cycle progression across land plants.

Materials and Methods

Plant culture

Physcomitrium patens (Hedw.) B.S.G. 'Gransden 2004' was cultured as previously described (57). Plants were grown on BCD (-AT) or BCD (AT) medium with 0.8% (w/v) agar at 25 °C under 16h-white light and 8h-dark conditions to generate protonema and gametophores materials. For protonema phenotyping, sterilized spores were germinated on cellophane-covered plates containing –AT or AT media, and photographed at 5, 7, 11 and 16 days. For unilateral light experiments, protonema filaments were displayed on cellophane-covered plates containing AT media and on the top two microscopy cover glasses to allow only unilateral growth of the protonema. Plates were then placed horizontally in a dark box for 7 weeks on which only a single side allowed light to penetrate. That side was covered with a plastic red wrapping to generate 660nm wavelength, which induces caulonema differentiation (33). For the NAA (1-Naphthaleneacetic acid, Sigma) experiments, sterilized spores were germinated on cellophane-covered plates containing –AT media supplied for 5µM of NAA (diluted in EtOH) during 10-15 days. To obtain sporophytes, plants at the gametophytic stage were transferred onto autoclaved Jiffy-7 (Jiffy Products International AS, Norway), half immersed in sterilized tap water and grown at 25°C for 15 days under 16h light and 8h dark conditions. Sporophyte formation was induced by incubation of gametophores at 15°C under 8h light and 16h dark cycle for at least 45 days (for the CRISPR lines, experiments were extended to 60 days due to a delay in sporophyte formation). Plants were submerged with sterilized tap water, replaced every week). For the NAA experiments, WT plants were watered with a tap water containing 25nM NAA, changed every week from the moment plants were transferred to the induction condition and till the end of the experiment (5 weeks after).

The *Columbia-0* (*Col-0*) ecotype of *Arabidopsis thaliana* was cultured on germination medium containing MS medium, at 22℃ under 16h light and 8h dark conditions. T-DNA lines used for complementation were obtained from the SALK genebank (*ntt*, SALK_007406; *wip4*, SALK_014672; *wip5,* SALK_114838 and *tt1-3* mutants, SALK_026171).

Protein sequence alignment and phylogenetic analysis

WIP protein sequences of *Arabidopsis thaliana, Physcomitrium patens*, *Marchantia polymorpha, Amborella trichopoda*, *Ginkgo biloba*, *Oryza sativa*, *Solanum lycopersicum*, *Vitis vinifera* and *Cucumis melo* were downloaded from Phytozome (https://phytozome-next.jgi.doe.gov/) and

Melonomics web site (https://www.melonomics.net/). The rest of the sequences were curated (only those proteins with a WIP motif) after a BLASTP analysis using the 1000 Plant Transcriptomes database (https://db.cngb.org/datamart/plant/DATApla4/) (Dataset S1) (23). Protein sequence alignment was computed by Mafft v7.526 (58), alignment trimming was done using ClipKit v2.11.4 (59) and phylogenetic tree inference was performed with IQ-Tree v2.4.0 (60)using the Phylogeny v2.0 pipeline (https://v2.phylogeny.fr/) (61)

P. patens plasmid constructs

To create the *PpWIP1-GUS* and *PpWIP2-GUS* translational fusion vectors, the plasmid *pGUS-NPTIILox* carrying the *GUS:tNOS* cassette from *PpCCD8pro:GUS* was cloned into the *pBNRF* plasmid (62,63). The *PpWIP1-GUS* knock-in cassette used to generate in-frame protein fusion of *PpWIP1* with the *GUS* bears a 923-bp 5' targeting fragment (chrom15: 11720915–11719993 in Phytozome) and a 983-bp 3' targeting fragment (chrom15: 11719989–11719006 in Phytozome) of the *WIP1* gene (gene ID *Pp3c15_17790*), flanking the *GUS:tNOS* and *pAct::Neo*^{R} cassettes from the *pGUS-NPTIILox* plasmid. *PpWIP1-GUS* was digested with *Not*I and *Apa*I for transformation. The *PpWIP2-GUS* knock-in cassette used to generate in-frame fusions of *PpWIP2* with the *GUS* bears a 894-bp 5' targeting fragment (chrom9: 15052029–15052922 in Phytozome) and a 998-bp 3' targeting fragment (chrom9: 15052926–15053923 in Phytozome) of the *WIP2* gene (gene ID *Pp3c9_22230*), flanking the *GUS:tNOS* and *pAct::Neo*^{R} cassettes from the *pGUS-NPTIILox* plasmid. *PpWIP2-GUS* was digested with *Not*I and *Apa*I for transformation.

Two series of, single *wip1* and *wip2* mutants and double *wip1wip2* mutants, were produced. The first one was based on a gene targeting strategy, using the *PpWIP1-rec* and *PpWIP2-rec* plasmids. The second one was based on the CRISPR-Cas9 system, using the *PpWIP1*-Δ and *PpWIP2*-Δ plasmids. To generate the plasmid PpWIP1-rec, a 1270-bp 5' targeting fragment (chrom15: 11723772–11722866 in Phytozome) and a 907-bp 3' targeting fragment (chrom15: 11719460–11718191 in Phytozome) were cloned in *pBHRF* (64). *PpWIP1-rec* was digested with *Hind*III and *Pac*I for transformation. To generate the *PpWIP2-rec*, a 964-bp 5' targeting fragment (chrom9: 15052893–15053856 in Phytozome) and an 888-bp 3' targeting fragment (chrom9: 15049765–15050652 in Phytozome) were cloned in *pBNRF. PpWIP2-rec* was digested with *Bam*HI and *Nsi*I for transformation. Plasmids *PpWIP1*-Δ and *PpWIP2*-Δ were generated as follows. Guide RNA (sgRNA) sequences specific to the *PpWIP1* or *PpWIP2* genes were chosen (Dataset S9) using the CRISPOR tool (https://crispor.gi.ucsc.edu/) (65). The sgRNA expression cassettes were cloned, using the GoldenBraid strategy (66), into a *pDGB3_alpha1* plasmid carrying a *35S::neoR* cassette from pBNRF. They comprise the promoter of the *P. patens* U6 snRNA (67), the 5'-G-$N_{(19)}$-3' guide

sequences targeting the *PpWIP1* or *PpWIP2* genes, the sgRNA scaffold and the SUP4 terminator (68).

P. patens transformation and selection procedures

P. patens protoplast isolation was performed from 6-day-old blended protonema tissue as previously described (57). To generate the *PpWIP1-GUS* and *PpWIP2-GUS* translational fusions and *wip1* and *wip2* mutants *P. patens* wild-type protoplasts were co-transfected using the linearized plasmids respectively. Transfected plants were selected with 25 mg/l hygromycin B (Duchefa) or with 30 mg/l G418 (Duchefa). Stable transformants were isolated following a second round before genotyping. To produce the *wip1wip2* double mutant, *wip1* and *wip2* plants were crossed and spores corresponding to the double *wip1wip2* mutants were selected on 25 mg/l hygromycin B plus 30 mg/l G418. To generate the *wip1*Δ, *wip2*Δ and double *wip1*Δ*wip2*Δ mutants (ATG to Stop deletion) *P. patens* wild-type protoplasts were co-transfected with the pUbi-Cas9 plasmid (69) and the *PpWIP1-ko*, *PpWIP2-ko* or *PpWIP1-ko* plus *PpWIP2-ko* plasmids, respectively. Transfected plants were selected with 30 mg/l G418 (Duchefa). Growing plants were individually isolated and subcultured on BCD (AT) medium before genotyping. Moss genomic DNA samples were isolated from 50 mg of fresh tissue as previously described (70). Targeted gene conversion events, corresponding to *wip1* and *wip2* and double *wip1wip2* recombinant mutants, as well as targeted gene deletion events, corresponding to *wip1*Δ*, wip2*Δ and double *wip1*Δ*wip2*Δ mutants, were identified using PCR primers described in Dataset S9.

Genotyping of _GUS_ lines and _wip_ recombinant mutants by Illumina

Genomic DNA was extracted from ~50 mg of fresh tissue from Pp*WIP1-GUS, PpWIP1-GUS* reporter lines; and *wip1*, *wip2* and *wip1wip2* recombinant mutants and wild-type strains. Equal amounts of DNA were used to generate libraries using the NextSeq 500/550 High Output kitv2,5 (150cycles) for Illumina and sequenced on the Nextseq500. Sequencing reads from the different datasets were trimmed using Cutadapt and subsequently aligned to the *P. patens* reference genome supplemented either with *PpWIP1-GUS* or *PpWIP1-GUS* vector sequences, using BWA-MEM2. The resulting alignments were filtered with samtools using the options "-F 3852 -q 50" to retain high-quality, properly paired reads. Reads supporting the insertion were then extracted from the alignments, confirming the integration of the vector sequence at a unique locus in the genome. Each putative insertion site or deletion of the gene in *wip* mutant lines were manually inspected in the Integrative Genomics Viewer (IGV).

Plasmid constructs for complementation and transformation of _A. thaliana_

Constructs used for complementation experiments were generated by amplifying promoter regions (*promAtWIP4* and *promNTT*) and full CDS (*PpWIP1*, *PpWIP2*, *NTT* and *AtWIP4*) with the Phusion High-Fidelity DNA polymerase (Thermo Scientific). Fragments of 4.1-kb for *promAtWIP4* and 4.6-kb for *promNTT* were inserted into a synthetic MultiSite Gateway-compatible entry vector pENTRY57_L4R1 (synthesized by ProteoGenix). The vector was first linearized using the BsaI cutting site (NEB # R0535) and then cloned using the ClonExpress® II One Step Cloning Kit (Vazyme). CDS of *NTT, AtWIP4*, *PpWIP1* and *PpWIP2* genes were inserted into a MultiSite Gateway entry vector *pDONR221* by using Gateway™ BP Clonase™ II Enzyme (Invitrogen). The *pH7m34GW* destination vector was used to generate final constructs by using the Gateway™ LR Clonase™ II Enzyme (Invitrogen) in combination with a vector containing the NosT sequence (*nost-P2RP3pGEMteasy*). To generate *promAtWIP4::AtWIP4*, *promAtWIP4::PpWIP1* and *promAtWIP4::PpWIP2*, segregating *nww* mutants (heterozygous for *NTT/ntt*) were transformed using *Agrobacterium tumefaciens* strain C58C1 by floral dip method, and primary transformants were selected on Hygromycin. Primers used for cloning are listed in Dataset S9. Complementation of *ntt* mutants was done using *promNTT:NTT*, *promNTT:PpWIP1* and *promNTT:PpWIP2* constructs using the same transformation method. The *promAtWIP4::GUS* and *promNTT::GUS* were constructed by fusing *AtWIP4* and *NTT* promoters in front of β-glucuronidase (*GUS-221pGEMteasy*) into the *pH7m34GW* destination vector (11).

Previously described cloning method was used to generate *promTT1::AtTT1*, *promTT1::PpWIP1* and *promTT1::PpWIP2* plasmids for complementation of the *transparent testa* phenotype *of tt1-3* mutants (12). After digestion with SpeI (New England, Biolabs), the promoter of *AtWIP1/TT1* was cloned into the pIJPB binary vector and confirmed by sequencing. CDS were amplified and cloned into *pDONR221*. *AtTT1, PpWIP1* and *PpWIP2* CDS were then introduced into the pIJPB plasmid by the Gateway® system (Invitrogen™). Primers used for cloning are listed in Dataset S9.

Vanillin staining and proanthocyanidin quantification

Vanillin staining and proanthocyanidin (PA) quantification were performed as previously described (12). Immature *Arabidopsis* seeds at the heart stage of embryogenesis were incubated for 30 min, in 1% (w/v) vanillin (4-Hydroxy-3-methoxybenzaldehyde; Sigma-Aldrich) prepared in 6 N hydrochloric acid, and subsequently visualized using a Leica macroscope. For PA quantification, ~10 mg of mature seeds was ground in acidic methanol. Acidic butanol and a ferric reagent were then added, and samples were boiled, cooled to room temperature, and centrifuged. The absorbance of the resulting supernatant was measured at 550 nm. PA content was determined by comparison with a cyanidin chloride (Sigma-Aldrich) standard curve.

Measurement of GUS Activity

Histochemical GUS assays were performed as described (71). Plants were grown from protonema on cellophane-covered plates containing –AT media. Samples were collected after 3 weeks and placed in 90% acetone for at least 1 day at -20°C. New formed protonema and gametophores from *WIP1*- and *WIP2-GUS* translational fusions were used.

Microscopy analysis

For GUS staining phenotyping, protonema size measurements, gametophores size and sporophytes phenotyping photographs were taken with a Zoom microscope (Azio Zoom.V16; Zeiss) equipped with an Axiocam camera (506 mono; Zeiss). For filament phenotyping, photographs were taken using a Nomarski microscope (BX53-DIC; Olympus) equipped with an Olympus camera (DP73, Olympus). For protonema and root phenotyping, plants were dissected and stained with the SCRI Renaissance 2200 (SR2200) dye (56) and images were obtained with a confocal laser scanning microscope (LSM880; Zeiss) using already described conditions (11). Image analyses were performed using ImageJ.

RT-qPCR analysis

To analyze the expression of the *PpWIP* genes, protonema of 11 days after sowing, as well as gametophyte apex after induction at 15°C, green and brown sporophytes, were sampled. Total RNAs were extracted with RNeasy plant kit (Qiagen, Germany) or Arcturus PicoPure RNA Isolation Kit (Applied Biosystems, USA), treated with DNase I (Qiagen, Germany), and subjected to first-strand cDNA synthesis using SuperScript™II RT (Invitrogen, Germany). RT products were used as templates in a PCR reaction using SYBR® Green no ROX Master kit (Eurogentec, Belgium). All PCR reactions were performed in a CFX96 real-time PCR system (Bio-Rad, USA). Quantitative RT-qPCR analysis was independently carried out in triplicate and the relative expression was calculated with the relative –ΔΔCt method using the gene *PpGAPDH* or *PpUBI1* as an internal control. All primer sets are listed in Dataset S9.

Determination of endogenous auxin

Spores of WT and *wip1wip2* mutants were germinated on cellophane-covered plates containing BCD(-AT) media, and incubated for 16 days. Endogenous auxin was determined by UPLC-ESI-MS/MS from 10 mg (dry weight) of 16-d-old protonema homogenized in liquid nitrogen (72). Indole-3-acetic acid-stable labelled isotopes were used as internal standards were prepared as previously described auxin extractions and measurements were carried out as previously described (73).

RNA-seq libraries and data analysis

Spores of *P. patens* WT, *wip1*, *wip2* and *wip1wip2* mutants were germinated on BCD (-AT) medium with cellophane and then sampled after 11 days. Total RNAs were extracted and treated with DNase I. RNA-seq libraries were prepared using NEBNext® Ultra™ II RNA Library Prep Kit with index oligo for each library (NEB, USA). Multiplex-sequencing was conducted on the HiSeq2000 platform (Illumina USA), and between 15 and 28 million read pairs per sample were obtained. To map raw reads to moss genome sequences with annotated gene models, genome assembly and gff annotation files of *Physcomitrium patens* v3.3 were obtained via the Phytozome website (http://www.phytozome.net). Reads were aligned to the genome sequences by using TopHat from CLC Genomics Workbench (http://www.clcbio.com/products/clc-genomics-workbench/) with the following options: "--segment-length 16", "--max-multihits 20", "--report-secondary-alignments", "--GTF Ppatens_152_gene_exons.gff3", and the other options set as default. Gene expression and differentially expressed (DE) genes were defined with the Deseq2 program (74). Deseq2 was run with default setting except "--min-alignment-count 1". Relative expression level was calculated in fragments per kilobase of exon model per million mapped reads (FPKM). Genes with q-value < 0.05 and abs(Log2FC) ≥ 1 were regarded as DE genes. Volcano plot, principal component analysis (PCA) and heatmaps were created using web tool VolcaNoseR (https://huygens.science.uva.nl/VolcaNoseR/) and ClustVis (https://biit.cs.ut.ee/clustvis_large/). GO analyses were performed in the PLAZA workbench (https://bioinformatics.psb.ugent.be/plaza/).

ampDAP-seq libraries and data analysis

For ampDAP-seq, c-terminal fragments of *PpWIP1* and *PpWIP2* CDS were cloned into the *pDONR222* using the Gateway™ BP Clonase™ Enzyme (Invitrogen) and then transferred into *pIX-HALO* using the Gateway™ LR Clonase™ II Enzyme (Invitrogen). Primers used for cloning and sequencing are listed in Table S1. Expression of *HALO-PpWIP1* and *HALO-PpWIP2* fusion proteins and generation of moss PCR-amplified genomic DNA libraries for protein binding were performed as previously described (38). DNA library sequencing on a NextSeq500 as 2 × 75 nt reads. ampDAP-Seq peaks and associated genes and motifs were predicted using a Snakemake pipeline (75). Qualities of the libraries were assessed with fastQC screen, adapters and low-quality bases were trimmed with cutadapt. Mapping was performed with Bowtie2 with parameters ("--very-sensitive -k 10"). The mapped files were filtered with samtools and peaks were predicted with genrich (https://github.com/jsh58/Genrich) with parameters ("-j -r"), and annotated with ChipSeeker bioconductor package (74). Motif discovery was done with Homer software and coverage tracks were generated with deeptools. CLC Genomics Workbench was used for visualization.

Electrophoretic mobility-shift assay

CDS sequences of PpWIP1 and PpWIP2 (in *pDONR221*) were cloned by the Gateway™ LR Clonase™ II Enzyme (Invitrogen) into the GST fusion vector *pDEST15* and introduced into *E. coli* strain *BL21* Rosetta. The *GST::PpWIPs* recombinant proteins or GST tag alone were induced in a 500-ml expression culture using 0.4 mM isopropyl β-D-1-thiogalactopyranoside, and cells were harvested 16 h after induction at 18°C. Cells were lysed using a combination of lysozyme treatment and sonication. The supernatant of the centrifuged lysate was used for GST-tag affinity purification using 0.5 ml Protino Glutathione Agarose 4B medium (Macherey-Nagel). Eluates were analyzed by SDS–PAGE and western blot. *PpYUCC* probe harboring the ampDAP-AtWIP5 motif was synthesized and labeled with biotin at their 5′ end. For probe competition, the unlabeled probe was added to the reactions. EMSA was performed using the LightShift chemiluminescent EMSA kit (Thermo Fisher Scientific, USA). Probe sequences are listed in Dataset S9.

Data availability

All data are available in the main paper or SI Appendix. Raw RNA-seq, DAP-seq data and sequencing data were deposited in the BioProject accession numbers PRJNA837469 (76), PRJNA994077 (77), and PRJNA1426583 (78), respectively.

Acknowledgments

This work was supported by AgreenSkills+ fellowship (WIPSCREEN, ID application: 1325, EU's Seventh Framework Programme FP7-609398, to MVGR); the PHC Maimonide program (42999PE, Campus France, to AB); the ERC NectarGland project (101095736, A.B.); the Saclay Plant Sciences-SPS (ANR-17-EUR-0007); the France 2030 program (ANR-22-PESV-0002, FN) and the IJPB's Plant Observatory technological platforms.

References

1. Graham LE, Cook ME, Busse JS. The origin of plants: body plan changes contributing to a major evolutionary radiation. Proc Natl Acad Sci U S A. 2000 Apr;97(9):4535–40. doi:10.1073/pnas.97.9.4535 PubMed PMID: 10781058.
2. Reski R. Development, Genetics and Molecular Biology of Mosses. Botanica Acta. 1998;111(1):1–15. doi:https://doi.org/10.1111/j.1438-8677.1998.tb00670.x
3. Ligrone R, Duckett JG, Renzaglia KS. The origin of the sporophyte shoot in land plants: a bryological perspective. Ann Bot. 2012 Oct 1;110(5):935–41. doi:10.1093/aob/mcs176
4. Panchy N, Lehti-Shiu M, Shiu SH. Evolution of Gene Duplication in Plants. Plant Physiol. 2016 Aug 1;171(4):2294–316. doi:10.1104/pp.16.00523
5. Appelhagen I, Lu GH, Huep G, Schmelzer E, Weisshaar B, Sagasser M. TRANSPARENT TESTA1 interacts with R2R3-MYB factors and affects early and late steps of flavonoid biosynthesis in the endothelium of Arabidopsis thaliana seeds. Plant Journal. 2011;67(3):406–19. doi:10.1111/j.1365-313X.2011.04603.x
6. Coen O, Magnani E. Seed coat thickness in the evolution of angiosperms. Cellular and Molecular Life Sciences. 2018;75(14):2509–18. doi:10.1007/s00018-018-2816-x

7. Crawford BCW, Ditta G, Yanofsky MF. The NTT Gene Is Required for Transmitting-Tract Development in Carpels of Arabidopsis thaliana. Current Biology. 2007;17(13):1101–8. doi:10.1016/j.cub.2007.05.079
8. Crawford BCW, Sewell J, Golembeski G, Roshan C, Long J, Yanofsky M. Genetic control of distal stem cell fate within root and embryonic meristems. Science. 2015;1(January):1–8. doi:10.1017/CBO9781107415324.004 PubMed PMID: 25246403.
9. Sagasser M, Lu GH, Hahlbrock K, Weisshaar B. A. thaliana Transparent testa 1 is involved in seed coat development and defines the WIP subfamily of plant zinc finger proteins. Genes Dev. 2002;16(1):138–49. doi:10.1101/gad.212702
10. Appelhagen I, Huep G, Lu GH, Strompen G, Weisshaar B, Sagasser M. Weird fingers: Functional analysis of WIP domain proteins. FEBS Lett. 2010;584(14):3116–22. doi:10.1016/j.febslet.2010.06.007
11. Du Y, Roldan MVG, Haraghi A, Haili N, Izhaq F, Verdenaud M, et al. Spatially expressed WIP genes control Arabidopsis embryonic root development. Nat Plants. 2022 Jun;8(6):635–45. doi:10.1038/s41477-022-01172-4 PubMed PMID: 35710883.
12. Roldan MVG, Izhaq F, Verdenaud M, Eleblu J, Haraghi A, Sommard V, et al. Integrative genome-wide analysis reveals the role of WIP proteins in inhibition of growth and development. Commun Biol. 2020;3(1):1–12. doi:10.1038/s42003-020-0969-2 PubMed PMID: 32415243.
13. Jones VAS, Dolan L. MpWIP regulates air pore complex development in the liverwort Marchantia polymorpha. Development (Cambridge). 2017;144(8):1472–6. doi:10.1242/dev.144287 PubMed PMID: 28174248.
14. Petricka JJ, Clay NK, Nelson TM. Vein patterning screens and the defectively organized tributaries mutants in Arabidopsis thaliana. Plant Journal. 2008;56(2):251–63. doi:10.1111/j.1365-313X.2008.03595.x
15. Martin A, Troadec C, Boualem A, Rajab M, Fernandez R, Morin H, et al. A transposon-induced epigenetic change leads to sex determination in melon. Nature. 2009;461(7267):1135–8. doi:10.1038/nature08498
16. Coudert Y, Novák O, Harrison CJ. A KNOX-Cytokinin Regulatory Module Predates the Origin of Indeterminate Vascular Plants. Current Biology. 2019 Aug 19;29(16):2743-2750.e5. doi:10.1016/j.cub.2019.06.083
17. Viaene T, Delwiche CF, Rensing SA, Friml J. Origin and evolution of PIN auxin transporters in the green lineage. Trends Plant Sci. 2013;18(1):5–10. doi:https://doi.org/10.1016/j.tplants.2012.08.009
18. Donoghue PCJ, Harrison CJ, Paps J, Schneider H. The evolutionary emergence of land plants. Current Biology. 2021;31(19):R1281–98. doi:10.1016/j.cub.2021.07.038 PubMed PMID: 34637740.
19. Bennett TA, Liu MM, Aoyama T, Bierfreund NM, Braun M, Coudert Y, et al. Plasma membrane-targeted PIN proteins drive shoot development in a moss. Current Biology. 2014;24(23):2776–85. doi:10.1016/j.cub.2014.09.054 PubMed PMID: 25448003.
20. Frank MH, Scanlon MJ. Transcriptomic evidence for the evolution of shoot meristem function in sporophyte-dominant land plants through concerted selection of ancestral gametophytic and sporophytic genetic programs. Mol Biol Evol. 2015 Feb 1;32(2):355–67. doi:10.1093/molbev/msu303 PubMed PMID: 25371433.
21. Szövényi P, Rensing SA, Lang D, Wray GA, Shaw AJ. Generation-biased gene expression in a bryophyte model system. Mol Biol Evol. 2011 Jan;28(1):803–12. doi:10.1093/molbev/msq254 PubMed PMID: 20855429.
22. Lin W, Wang Y, Coudert Y, Kierzkowski D. Leaf Morphogenesis: Insights From the Moss Physcomitrium patens. Front Plant Sci [Internet]. 2021;Volume 12-2021. Available from: https://www.frontiersin.org/journals/plant-science/articles/10.3389/fpls.2021.736212
23. Leebens-Mack JH, Barker MS, Carpenter EJ, Deyholos MK, Gitzendanner MA, Graham SW, et al. One thousand plant transcriptomes and the phylogenomics of green plants. Nature. 2019;574(7780):679–85. doi:10.1038/s41586-019-1693-2
24. Goodstein DM, Shu S, Howson R, Neupane R, Hayes RD, Fazo J, et al. Phytozome: a comparative platform for green plant genomics. Nucleic Acids Res. 2012 Jan 1;40(D1):D1178–86. doi:10.1093/nar/gkr944
25. Ren G, Li L, Huang Y, Wang Y, Zhang W, Zheng R, et al. GhWIP2, a WIP zinc finger protein, suppresses cell expansion in Gerbera hybrida by mediating crosstalk between gibberellin, abscisic acid, and auxin. New Phytologist. 2018;219(2):728–42. doi:10.1111/nph.15175
26. Zhang S, Tan FQ, Chung CH, Slavkovic F, Devani RS, Troadec C, et al. The control of carpel determinacy pathway leads to sex determination in cucurbits. Science (1979). 2022 Nov 4;378(6619):543–9. doi:10.1126/science.add4250

27. Kofuji R, Hasebe M. Eight types of stem cells in the life cycle of the moss Physcomitrella patens. Curr Opin Plant Biol. 2014;17(1):13–21. doi:10.1016/j.pbi.2013.10.007 PubMed PMID: 24507489.
28. Cove DJ, Perroud P françois, Charron AJ, Mcdaniel SF, Khandelwal A, Quatrano RS. A Novel Model System for Plant Development and Genomic Studies. In: Knight C, Perroud PF, Cove D, editors. The Moss Physcomitrella patens. Annual Pla. Wiley-Blackwell; 209AD. p. 69–104.
29. Vidali L, Bezanilla M. Physcomitrella patens: A model for tip cell growth and differentiation. Curr Opin Plant Biol. 2012;15(6):625–31. doi:10.1016/j.pbi.2012.09.008 PubMed PMID: 23022392.
30. Thelander M, Landberg K, Sundberg E. Auxin-mediated developmental control in the moss Physcomitrella patens. J Exp Bot. 2018;69(2):277–90. doi:10.1093/jxb/erx255 PubMed PMID: 28992074.
31. Ortiz-Ramírez C, Hernandez-Coronado M, Thamm A, Catarino B, Wang M, Dolan L, et al. A Transcriptome Atlas of Physcomitrella patens Provides Insights into the Evolution and Development of Land Plants. Mol Plant. 2016;9(2):205–20. doi:10.1016/j.molp.2015.12.002 PubMed PMID: 26687813.
32. Fernandez-Pozo N, Haas FB, Meyberg R, Ullrich KK, Hiss M, Perroud PF, et al. PEATmoss (Physcomitrella Expression Atlas Tool): a unified gene expression atlas for the model plant Physcomitrella patens. Plant Journal. 2020. 165–177 p. doi:10.1111/tpj.14607 PubMed PMID: 31714620.
33. Miyazaki S, Nakajima M, Kawaide H. Assays of Protonemal Growth Responses in Physcomitrella patens Under Blue- and Red-Light Stimuli BT - Phototropism: Methods and Protocols. In: Yamamoto KT, editor. New York, NY: Springer New York; 2019. p. 35–43. Available from: https://doi.org/10.1007/978-1-4939-9015-3_4 doi:10.1007/978-1-4939-9015-3_4
34. Longton RE. Polysety in the British Bryophyta. Transactions of the British Bryological Society. 1962 Jul 1;4(2):326–33. doi:10.1179/tbbs.1962.4.2.326
35. Hughes JG. The occurrence of polysety in relation to the number of archegonia in the female inflorescences of Phascum cuspidatum Hedw. J Bryol. 1979 Jan 1;10(4):553–60. doi:10.1179/jbr.1979.10.4.553
36. Stark LR. Phenology and its Repercussions on the Reproductive Ecology of Mosses. Bryologist. 2002 Jun 1;105(2):204–18. doi:10.1639/0007-2745(2002)105[0204:PAIROT]2.0.CO;2
37. Chen Z, Wang W, Zhou S, Ding L, Xu Z, Sun X, et al. Single-cell RNA sequencing reveals dynamics of gene expression for 2D elongation and 3D growth in Physcomitrium patens. Cell Rep. 2024 Aug 27;43(8). doi:10.1016/j.celrep.2024.114524 PubMed PMID: 39046878.
38. Bartlett A, O'Malley RC, Huang S shan C, Galli M, Nery JR, Gallavotti A, et al. Mapping genome-wide transcription-factor binding sites using DAP-seq. Nat Protoc. 2017 Aug 20;12(8):1659–72. doi:10.1038/nprot.2017.055
39. O'Malley RC, Huang SSC, Song L, Lewsey MG, Bartlett A, Nery JR, et al. Cistrome and Epicistrome Features Shape the Regulatory DNA Landscape. Cell. 2016;165(5):1280–92. doi:10.1016/j.cell.2016.04.038 PubMed PMID: 27203113.
40. Jang G, Yi K, Pires ND, Menand B, Dolan L. RSL genes are sufficient for rhizoid system development in early diverging land plants. Development. 2011;138(11):2273–81. doi:10.1242/dev.060582 PubMed PMID: 21558375.
41. Steffen JG, Kang IH, Portereiko MF, Lloyd A, Drews GN. AGL61 interacts with AGL80 and is required for central cell development in Arabidopsis. Plant Physiol. 2008;148(1):259–68. doi:10.1104/pp.108.119404 PubMed PMID: 18599653.
42. Werner T, Motyka V, Laucou V, Smets R, Onckelen H Van, Schmülling T. Cytokinin-Deficient Transgenic Arabidopsis Plants Show Multiple Developmental Alterations Indicating Opposite Functions of Cytokinins in the Regulation of Shoot and Root Meristem Activity. Source: The Plant Cell [Internet]. 2003. Available from: www.plantcell.org/cgi/doi/10.1
43. Booker J, Auldridge M, Wills S, Mccarty D, Klee H, Leyser O. MAX3/CCD7 Is a Carotenoid Cleavage Dioxygenase Required for the Synthesis of a Novel Plant Signaling Molecule. Current Biology. 2004;14:1232–8. doi:10.1016/j
44. Landberg K, Šimura J, Ljung K, Sundberg E, Thelander M. Studies of moss reproductive development indicate that auxin biosynthesis in apical stem cells may constitute an ancestral function for focal growth control. New Phytologist. 2021 Jan 1;229(2):845–60. doi:10.1111/nph.16914 PubMed PMID: 32901452.
45. Lavy M, Prigge MJ, Tao S, Shain S, Kuo A, Kirchsteiger K, et al. Constitutive auxin response in Physcomitrella reveals complex interactions between Aux/IAA and ARF proteins. Elife. 2016;5(JUN2016):1–22. doi:10.7554/eLife.13325 PubMed PMID: 27247276.

46. Perroud PF, Haas FB, Hiss M, Ullrich KK, Alboresi A, Amirebrahimi M, et al. The Physcomitrella patens gene atlas project: large-scale RNA-seq based expression data. Plant Journal. 2018;95(1):168–82. doi:10.1111/tpj.13940 PubMed PMID: 29681058.
47. Whitewoods CD, Cammarata J, Nemec Venza Z, Sang S, Crook AD, Aoyama T, et al. CLAVATA Was a Genetic Novelty for the Morphological Innovation of 3D Growth in Land Plants. Current Biology. 2018;28(15):2365-2376.e5. doi:10.1016/j.cub.2018.05.068 PubMed PMID: 30033333.
48. Kong L, Liu Y, Zhi P, Wang X, Xu B, Gong Z, et al. Origins and Evolution of Cuticle Biosynthetic Machinery in Land Plants . Plant Physiol. 2020 Dec 1;184(4):1998–2010. doi:10.1104/pp.20.00913
49. O'Donoghue MT, Chater C, Wallace S, Gray JE, Beerling DJ, Fleming AJ. Genome-wide transcriptomic analysis of the sporophyte of the moss Physcomitrella patens. J Exp Bot. 2013;64(12):3567–81. doi:10.1093/jxb/ert190
50. Sigel EM, Schuettpelz E, Pryer KM, Der JP. Overlapping patterns of gene expression between gametophyte and sporophyte phases in the fern polypodium amorphum (Polypodiales). Front Plant Sci. 2018 Oct 9;9. doi:10.3389/fpls.2018.01450
51. Wallner ES, Edelbacher N, Dolan L. De novo meristem development in Marchantia polymorpha requires light and an apical auxin signaling minimum. Current Biology. 2026 Jan 19;36(2):278-289.e5. doi:10.1016/j.cub.2025.11.016
52. Flores-Sandoval E, Suzuki H, Lazner JA, Briginshaw LN, Fisher TJ, Romani F, et al. The B-class auxin response factor MpARF2 is essential for meristem organization in free-living plant gametophytes. Current Biology. 2026 Jan 19;36(2):261-277.e8. doi:10.1016/j.cub.2025.11.015
53. Landberg K, Pederson ERA, Viaene T, Bozorg B, Friml J, Jönsson H, et al. The moss physcomitrella patens reproductive organ development is highly organized, affected by the two SHI/STY genes and by the level of active auxin in the SHI/STY expression domain. Plant Physiol. 2013;162(3):1406–19. doi:10.1104/pp.113.214023 PubMed PMID: 23669745.
54. Véron E, Vernoux T, Coudert Y. Phyllotaxis from a Single Apical Cell. Trends Plant Sci. 2021 Feb 1;26(2):124–31. doi:10.1016/j.tplants.2020.09.014
55. Thelander M, Landberg K, Muller A, Cloarec G, Cunniffe N, Huguet S, et al. Apical dominance control by TAR-YUC-mediated auxin biosynthesis is a deep homology of land plants. Current Biology. 2022 Sep 12;32(17):3838-3846.e5. doi:10.1016/j.cub.2022.06.064
56. Mutte SK, Kato H, Rothfels C, Melkonian M, Wong GKS, Weijers D. Origin and evolution of the nuclear auxin response system. Yu H, editor. Elife. 2018;7:e33399. doi:10.7554/eLife.33399
57. Charlot F, Goudounet G, Nogué F, Perroud PF. Physcomitrium patens Protoplasting and Protoplast Transfection. In: Wang K, Zhang F, editors. Protoplast Technology: Methods and Protocols [Internet]. New York, NY: Springer US; 2022. p. 3–19. Available from: https://doi.org/10.1007/978-1-0716-2164-6_1 doi:10.1007/978-1-0716-2164-6_1
58. Katoh K, Standley DM. MAFFT multiple sequence alignment software version 7: Improvements in performance and usability. Mol Biol Evol. 2013 Apr;30(4):772–80. doi:10.1093/molbev/mst010 PubMed PMID: 23329690.
59. Steenwyk JL, Buida TJ, Li Y, Shen XX, Rokas A. ClipKIT: A multiple sequence alignment trimming software for accurate phylogenomic inference. PLoS Biol. 2020 Dec 2;18(12). doi:10.1371/journal.pbio.3001007 PubMed PMID: 33264284.
60. Minh BQ, Schmidt HA, Chernomor O, Schrempf D, Woodhams MD, Von Haeseler A, et al. IQ-TREE 2: New Models and Efficient Methods for Phylogenetic Inference in the Genomic Era. Mol Biol Evol. 2020 May 1;37(5):1530–4. doi:10.1093/molbev/msaa015 PubMed PMID: 32011700.
61. Dereeper A, Guignon V, Blanc G, Audic S, Buffet S, Chevenet F, et al. Phylogeny.fr: robust phylogenetic analysis for the non-specialist. Nucleic Acids Res. 2008;36(Web Server issue). doi:10.1093/nar/gkn180 PubMed PMID: 18424797.
62. Schaefer DG, Cell P. Principles and protocols to work with the moss Physcomitrella patens. Plant Cell. 1998;(September):1–13.
63. Proust H, Hoffmann B, Xie X, Yoneyama K, Schaefer DG, Yoneyama K, et al. Strigolactones regulate protonema branching and act as a quorum sensing-like signal in the moss Physcomitrella patens. Development. 2011 Apr 15;138(8):1531–9. doi:10.1242/dev.058495
64. Schaefer DG, Delacote F, Charlot F, Vrielynck N, Guyon-Debast A, Le Guin S, et al. RAD51 loss of function abolishes gene targeting and de-represses illegitimate integration in the moss Physcomitrella patens. DNA Repair (Amst). 2010;9(5):526–33. doi:https://doi.org/10.1016/j.dnarep.2010.02.001
65. Concordet JP, Haeussler M. CRISPOR: Intuitive guide selection for CRISPR/Cas9 genome editing experiments and screens. Nucleic Acids Res. 2018 Jul 2;46(W1):W242–5. doi:10.1093/nar/gky354 PubMed PMID: 29762716.

66. Sarrion-Perdigones A, Vazquez-Vilar M, Palací J, Castelijns B, Forment J, Ziarsolo P, et al. GoldenBraid 2.0: A Comprehensive DNA Assembly Framework for Plant Synthetic Biology . Plant Physiol. 2013 Jul 1;162(3):1618–31. doi:10.1104/pp.113.217661
67. Collonnier C, Epert A, Mara K, Maclot F, Guyon-Debast A, Charlot F, et al. CRISPR-Cas9-mediated efficient directed mutagenesis and RAD51-dependent and RAD51-independent gene targeting in the moss Physcomitrella patens. Plant Biotechnol J. 2017 Jan 1;15(1):122–31. doi:https://doi.org/10.1111/pbi.12596
68. Phane Ché Din S, Riva M, Schultz P, Sentenac A, Carles C. The RNA cleavage activity of RNA polymerase III is mediated by an essential TFIIS-like subunit and is important for transcription termination [Internet]. 1998. Available from: www.genesdev.org
69. Perroud PF, Guyon-Debast A, Casacuberta JM, Paul W, Pichon JP, Comeau D, et al. Improved prime editing allows for routine predictable gene editing in Physcomitrium patens. J Exp Bot. 2023 Oct 13;74(19):6176–87. doi:10.1093/jxb/erad189
70. Lopez-Obando M, Hoffmann B, Géry C, Guyon-Debast A, Téoulé E, Rameau C, et al. Simple and efficient targeting of multiple genes through CRISPR-Cas9 in Physcomitrella patens. G3: Genes, Genomes, Genetics. 2016;6(11):3647–53. doi:10.1534/g3.116.033266
71. Dedow LK, Oren E, Braybrook SA. Fake news blues: A GUS staining protocol to reduce false-negative data. Plant Direct. 2022 Feb 1;6(2). doi:10.1002/pld3.367
72. Le Roux C, Del Prete S, Boutet-Mercey S, Perreau F, Balagué C, Roby D, et al. The hnRNP-Q Protein LIF2 Participates in the Plant Immune Response. PLoS One [Internet]. 2014 Jun 10;9(6):e99343. Available from: https://doi.org/10.1371/journal.pone.0099343
73. Ligerot Y, de Saint Germain A, Waldie T, Troadec C, Citerne S, Kadakia N, et al. The pea branching RMS2 gene encodes the PsAFB4/5 auxin receptor and is involved in an auxin-strigolactone regulation loop. PLoS Genet. 2017 Dec 8;13(12):e1007089–e1007089. doi:10.1371/journal.pgen.1007089
74. Yu G, Wang LG, He QY. ChIPseeker: an R/Bioconductor package for ChIP peak annotation, comparison and visualization. Bioinformatics. 2015 Jul;31(14):2382–3. doi:10.1093/bioinformatics/btv145 PubMed PMID: 25765347.
75. Köster J, Rahmann S. Snakemake—a scalable bioinformatics workflow engine. Bioinformatics. 2018 Oct 15;34(20):3600. doi:10.1093/bioinformatics/bty350
76. MV Gomez Roldan. *Physcomitrium patens* protonema. National Center for Biotechnology Information (NCBI). https://www.ncbi.nlm.nih.gov/search/all/?term=PRJNA837469. Deposited 26 April 2023.
77. MV Gomez Roldan. DAP-seq *Physcomitrium patens*. National Center for Biotechnology Information (NCBI). https://www.ncbi.nlm.nih.gov/search/all/?term=PRJNA994077. Deposited 12 May 12 2022.
78. MV Gomez Roldan. Sequencing Physcomitrium lines. National Center for Biotechnology Information (NCBI). https://www.ncbi.nlm.nih.gov/search/all/?term=PRJNA1426583. Deposited 23 January 2026.

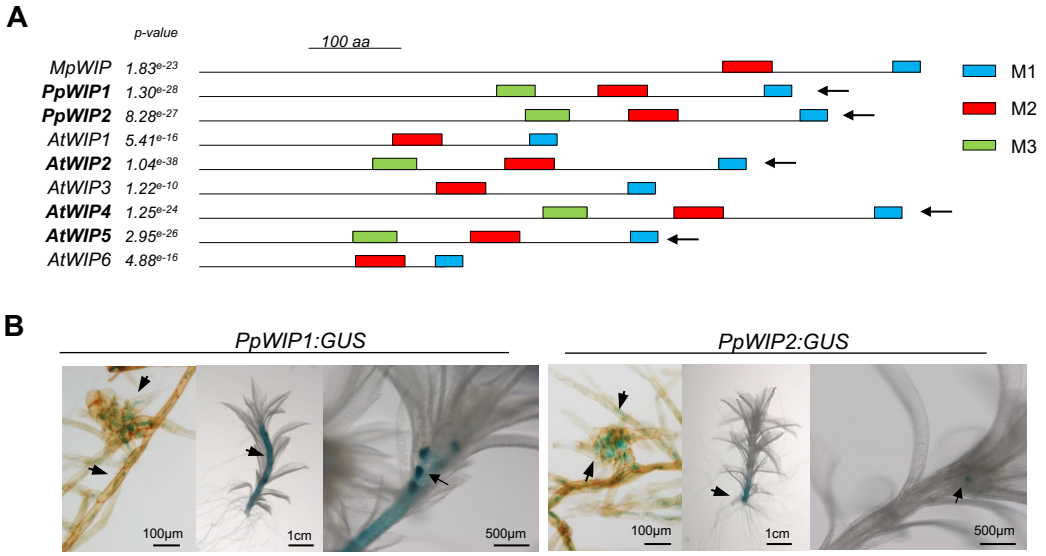

Figure 1. Structure of WIP proteins and expression patterns of *Physcomitrium patens* WIPs. A) MEME motif analysis using the N-terminal part of the WIP proteins. All the WIP proteins share M1 (blue) and M2 (red) motifs. PpWIP1 and PpWIP2 share the M3 motif (green) with AtWIP2, AtWIP4 and AtWIP5. AtWIP1, AtWIP3 and AtWIP6 and MpWIP lack the M3 motif. *p*-value provided by MEME software represent the probability that a random sequence would have a match to the motif under test. B) GUS staining of PpWIP1-GUS and PpWIP2-GUS gametophores. Arrows mark GUS signal. PpWIP1-GUS shows strong expression in developing and adult gametophyte thalli after 4 weeks under sporulation conditions (15 °C), whereas PpWIP2-GUS displays weaker expression mainly in developing gametophytes. No sporophytes were observed.

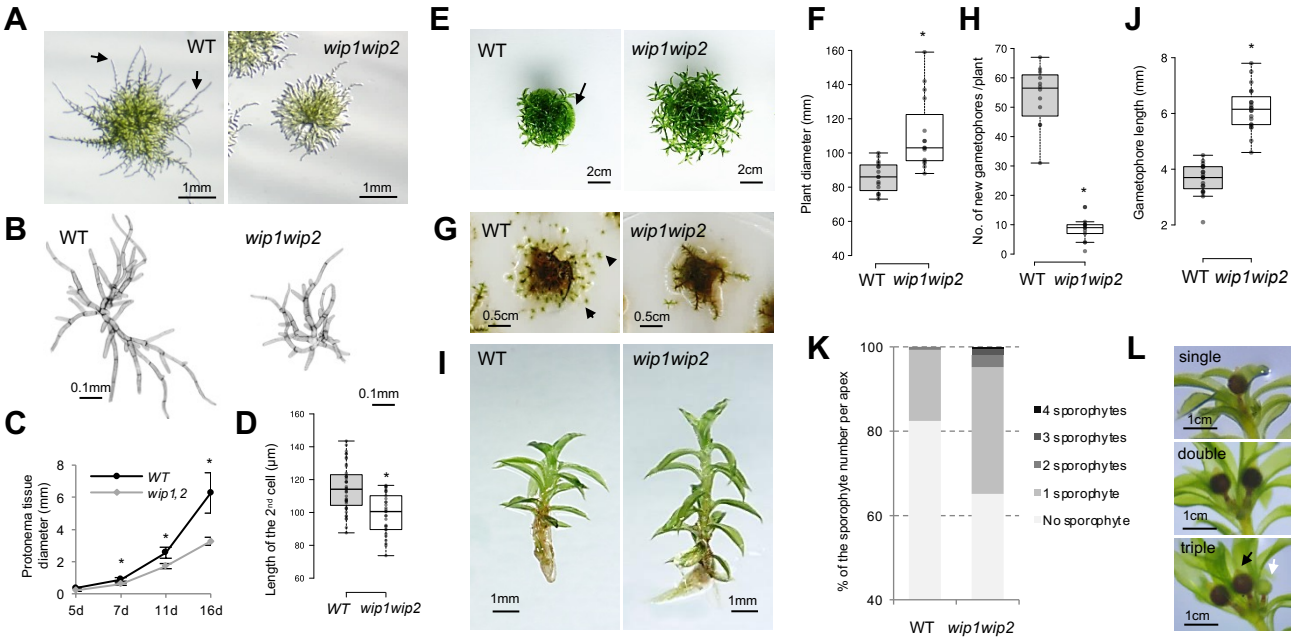

Figure 2. PpWIPs regulate the chloronema-to-caulonema transition and polysety. A) Overview of WT and *wip1wip2* double mutant protonema tissue germinated from spores, grown on the –AT medium with cellophane under white light for 11 days. Black arrows represent caulonema filaments. B) Confocal overview of the reduced protonema development in *wip1wip2* protonema at 7 day after germination compared to WT. C) Protonema growth in WT and *wip1wip2* double mutant during 16 days, measured by the diameter of the protonema tissue (n = 10; bars = s.d.; Student's t test *p<0.01). D) Length of the second cell in protonema tissue of 7 days (n = 30; bars = s.d.; Student's t test *p<0.01). E) Overview of 3-week-old WT and *wip1wip2* plants grown on the +AT medium. Black arrow indicates the presence of protonema in WT plants. F) Size of the plant at 3-week-old (n = 15; bars = s.d.; Student's t test *p<0.1). G) Overview of 2-month-old WT and *wip1wip2* plants grown on the –AT medium. H) Number of newly formed gametophores from the plant after the 2-month culture (n = 13; bars = s.d.; Student's t test *p<0.01). I) Overview of WT and *wip1wip2* gametophores formed from the 3-week-old plants grown on the +AT medium. J) Length of WT and *wip1wip2* gametophores formed from the 3-week-old plants grown on the +AT medium (n = 20; bars = s.d.; Student's t test *p<0.01). K) Proportion of apexes with none, one or more sporophytes in WT and *wip1wip2* double mutant. Two hundred apexes were dissected per genotype from plants grown under induced condition for 2 months (note that y axis start at 40% for better visibility of the differences between genotypes). L) Single, double and triple sporophytes at the apex of *wip1wip2* gametophores. Black arrow: a brown sporophyte; white arrow: a green sporophyte.

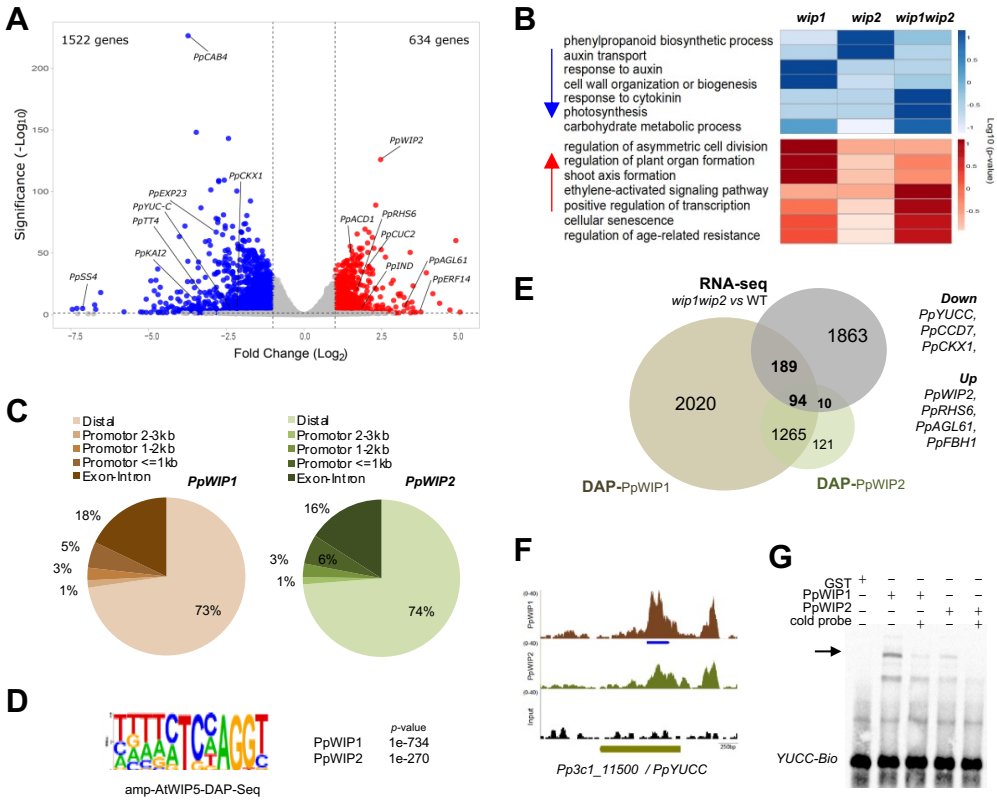

Figure 3. Putative targeted genes of PpWIPs. A) Volcano plot showing the differential expressed genes (blue dots, down-regulated; red dots, up-regulated) between WT and *wip1wip2* protonema (RNA-seq, |Log2FC| ≥1, FDR <0.05). B) GO analysis of the down-regulated genes in *wip1*, *wip2* and *wip1wip2* samples (compared to WT). Venn diagram showing the overlap of downregulated genes on *wip1*, *wip2* and *wip1wip2* compared to WT. C) Distribution of peaks bound by the C-terminal PpWIP1 and PpWIP2 proteins (DAP-seq). D) The "AtWIP5" binding motif, previously identified from the ampDAP-seq dataset, is present in the PpWIP-ampDAP-seq dataset. E) Venn diagram showing the overlap of genes found in DAP-seq (PpWIP1 and PpWIP2) that are significant different in the RNA-seq of *wip1wip2* protonema. Representative up- and down-regulated genes are shown. F) Peaks found in PpWIP1 and PpWIP2 DAP-seq datasets in the *PpYUCC locus*. G) EMSA experiment showing PpWIP1 and PpWIP2 proteins bind to Pp*YUCC* gene sequence. Red arrow shows the retard of the PpWIPs proteins with the biotinylated probe. Unlabeled probes (20 pmol) were used for the binding competition assay (cold probe). GST was used as the negative control.

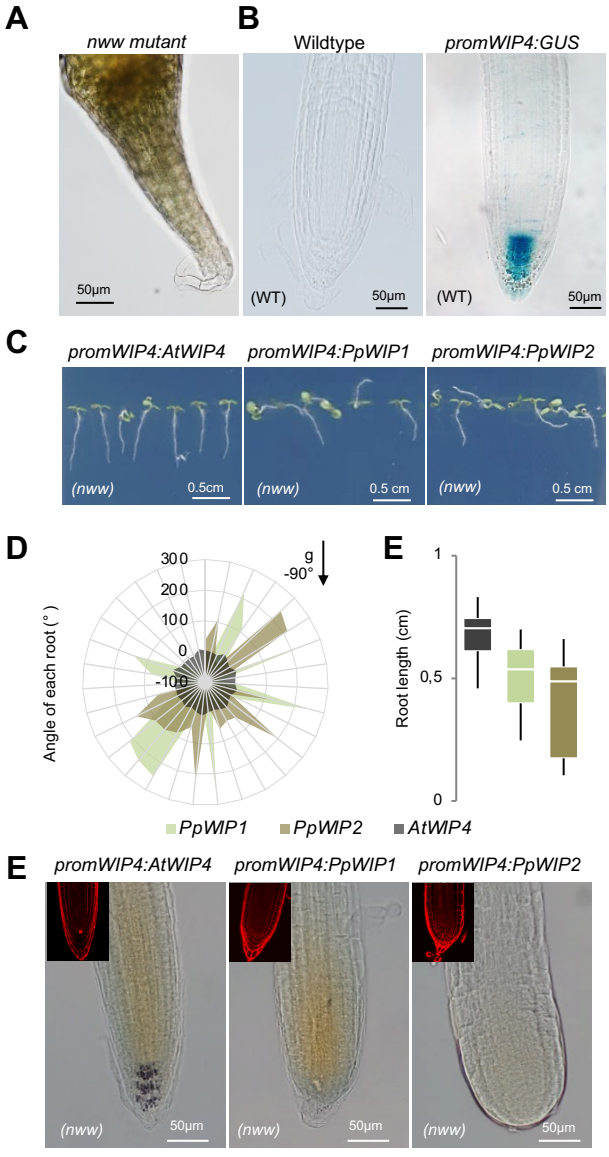

Figure 4. Targeted expression of Pp*WIP*s in *nww* roots. A) The rootless phenotype of *nww* mutants. B) *promWIP4:GUS* expression in distal root of WT, including QC, columella initial and columella. C) Overview of 6 days-post-germination (d.p.g.) *nww* roots complemented with *promWIP4:WIP4*, *promWIP4:PpWIP1* and *promWIP4:PpWIP2*. D) Gravitropic response in *nww* roots complemented with *promWIP4:PpWIP1*, *promWIP4:PpWIP2* compared to *promWIP4:WIP4* (*n*= 20). E) Root length of 6 dpg *nww* seedlings complemented with *promWIP4:PpWIP1*, *promWIP4:PpWIP2* and *promWIP4:WIP4* (*n* = 20, bars = SD). F) Lugol staining of amyloplasts in 6 dpg *nww* columella complemented with *promWIP4:WIP4*, *promWIP4:PpWIP1* and *promWIP4:PpWIP2*.

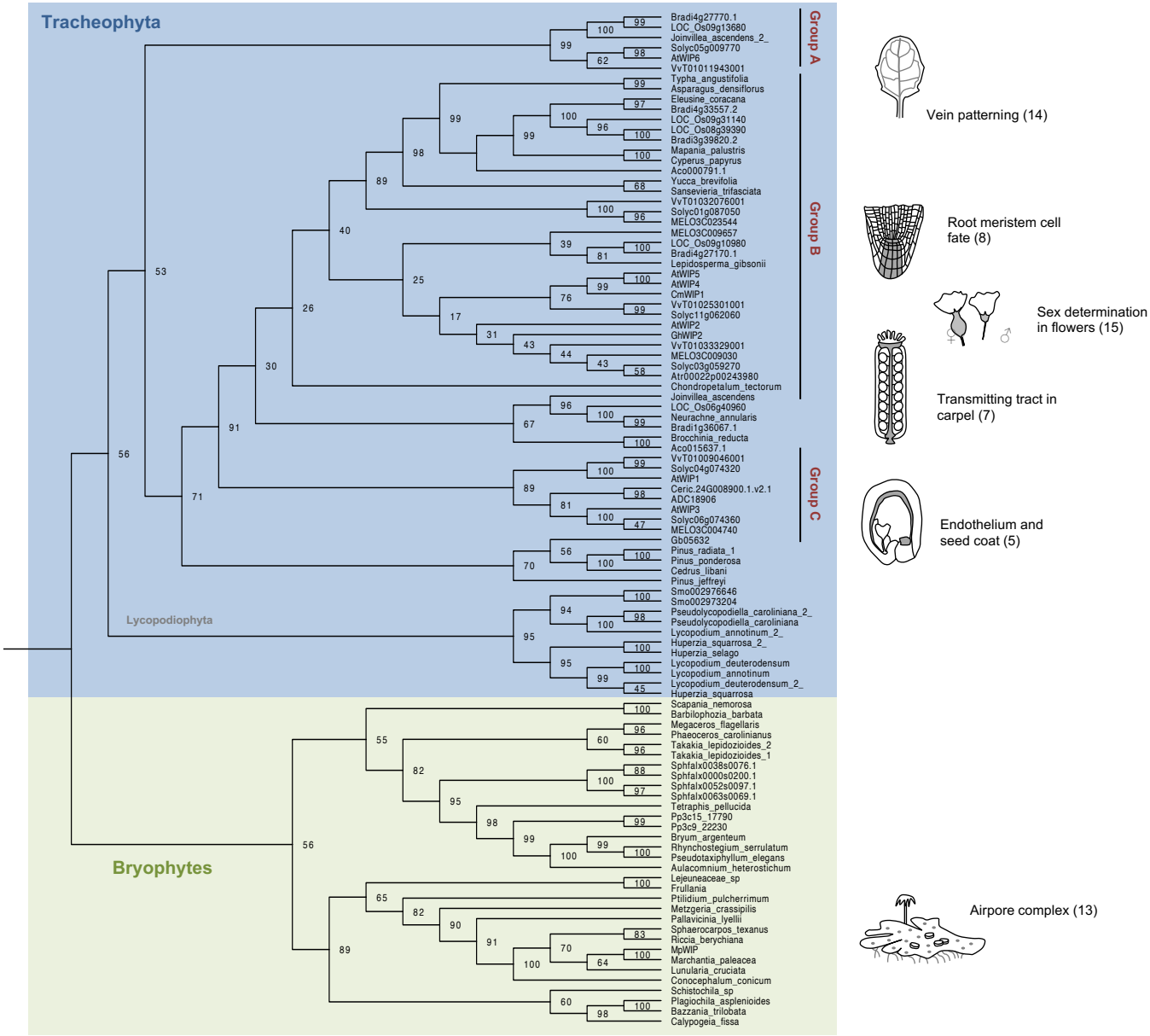

Figure S1. Maximum-likelihood phylogeny of WIP proteins across land plants. The tree was inferred using a maximum-likelihood approach. Major lineages are indicated by background shading (bryophytes in green; lycophytes in grey and vascular plants in blue). The two *Physcomitrium patens* WIP genes (*Pp3c9_22230* and *Pp3c15_17790*) likely result from a lineage-specific duplication. Three major clades recovered within vascular plants are indicated as Clades A–C. Bootstrap support values are shown at nodes. Where available, experimentally characterized functions of selected WIP genes are indicated, including roles in air pore complex development in *Marchantia polymorpha*, leaf vein patterning, transmitting tract development, root meristem regulation, and seed endothelium formation in *Arabidopsis thaliana*, as well as sex determination in *Cucumis melo*. The complete list of sequences used is provided in Dataset S1.

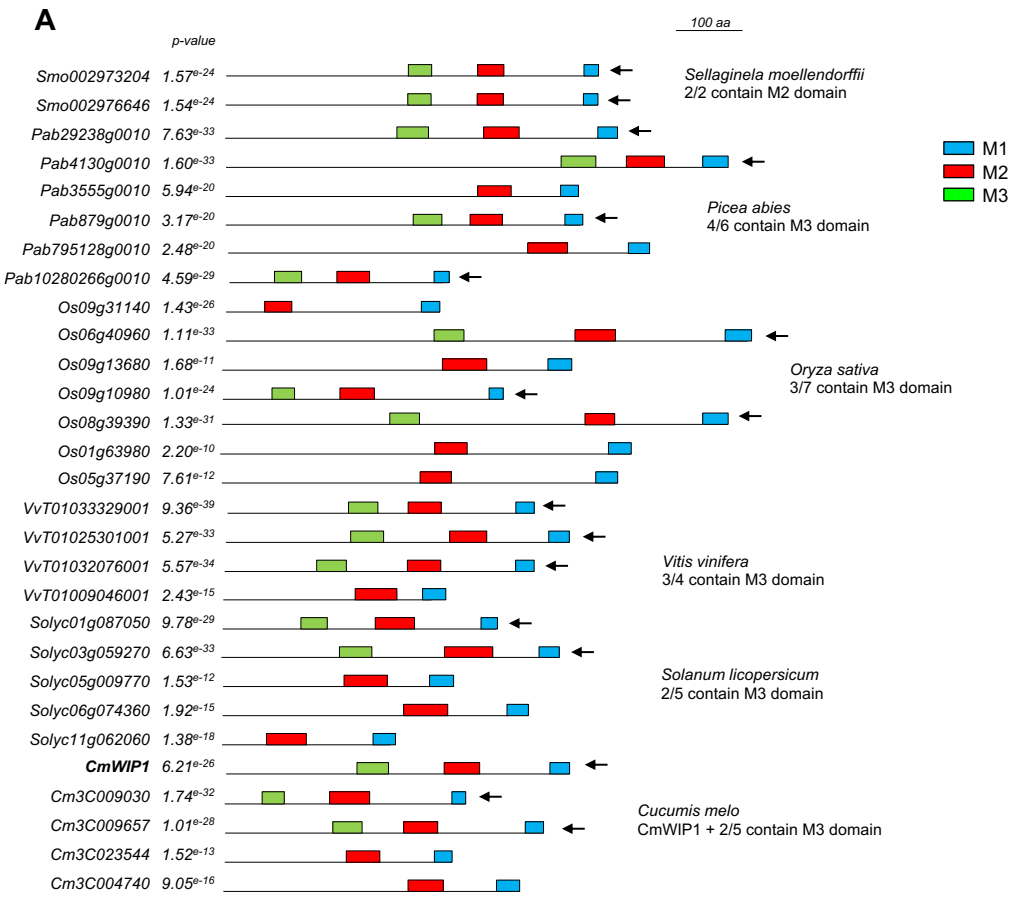

Figure S2. MEME motif analysis using the N-terminal part of the WIP proteins. MEME motif analysis using the N-terminal part of the WIP proteins. *p*-value provided by MEME software represent the probability that a random sequence would have a match to the motif under test. WIPs from *Marchantia polymorpha*, *Physcomitrium patens*, *Selaginella moellendorffii*, *Picea abies*, *Oryza sativa*, *Vitis vinifera, Solanum lycopersicum* and *Cucumis melo* all present the conserved M1 (blue) and M2 (red) motifs (expect for a WIP copy of *G. biloba* that do not show the red motif). Motif M3 (green) is present in some copies within each specie.

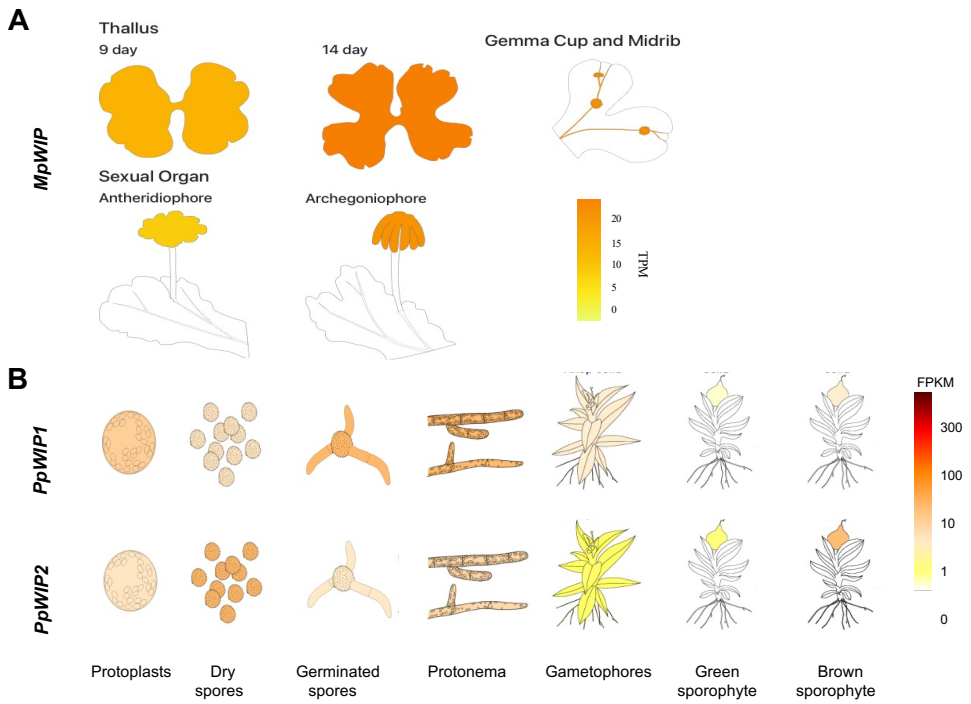

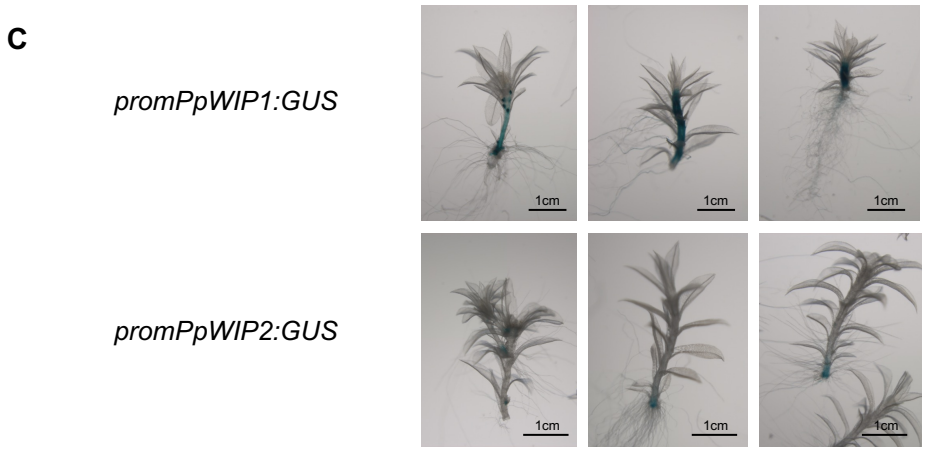

Figure S3. Expression of *PpWIPs* and *MpWIP* genes in databases. A) Expression of *MpWIP* (*Mp1g09500)* obtained from MarpolBase Genome Database for *Marchantia polymorpha* - *https://marchantia.info*. B) Expression of *PpWIP1 and PpWIP2* in protoplasts, spores, germinated spores, protonema, gametophyte and sporophytes of *P. patens* based on PEATMoss database. (https://peatmoss.plantcode.cup.uni-freiburg.de/). Data from sporophyte was obtained from Reute ecotype whereas other data are from Gransden ecotype. C) Additional pictures of GUS reporter lines presented in Fig. 1B.

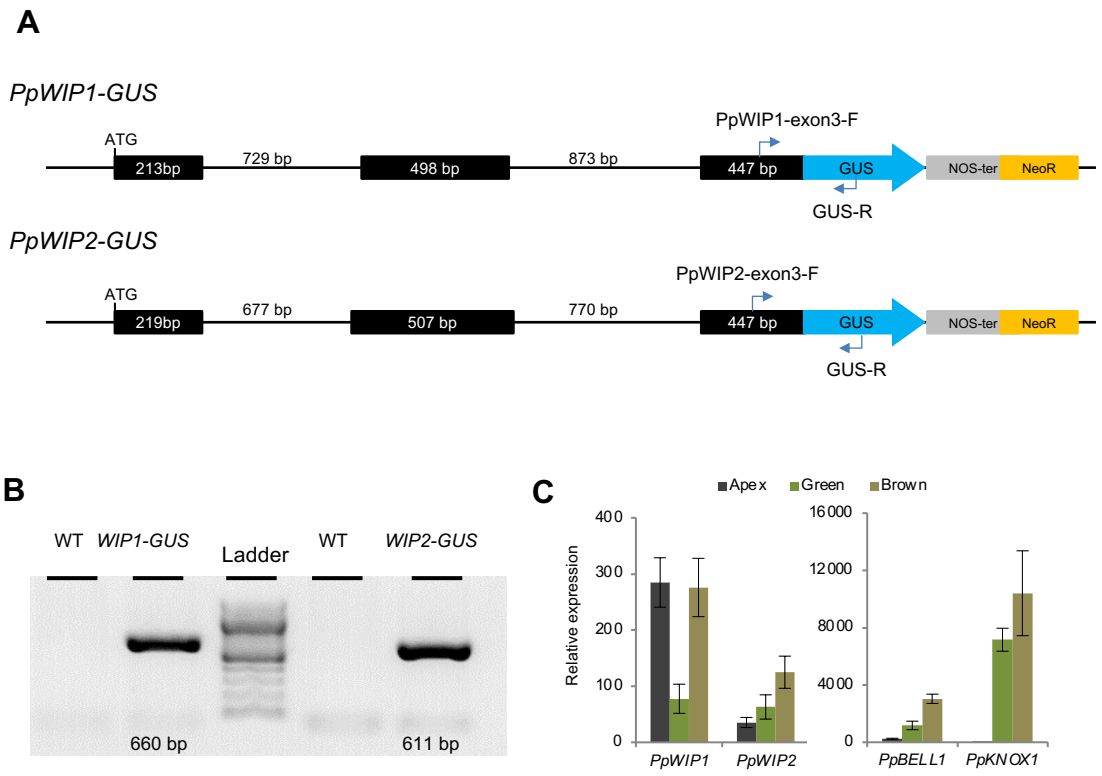

Figure S4. Construction of *PpWIP-GUS* fusion lines. A) Scheme of Pp*WIP1* and Pp*WIP2* loci and the GUS insertion. Arrows represent approximate positions of the forward and reverse primers to detect the insertion. B) PCR validation of the *PpWIP1-GUS* and *PpWIP2-GUS* lines. Expected size is indicated. C) Relative expression of *PpWIP1* and *PpWIP2* in gametophore apices and sporophyte tissues. Apex, gametophore tip 15 days after induction at 15 °C; Green, immature sporophyte; Brown, mature sporophyte. *PpBELL1* and *PpKNOX1* were used as sporophyte markers (n = 3 biological replicates, bars = SD; Gransden ecotype).

A

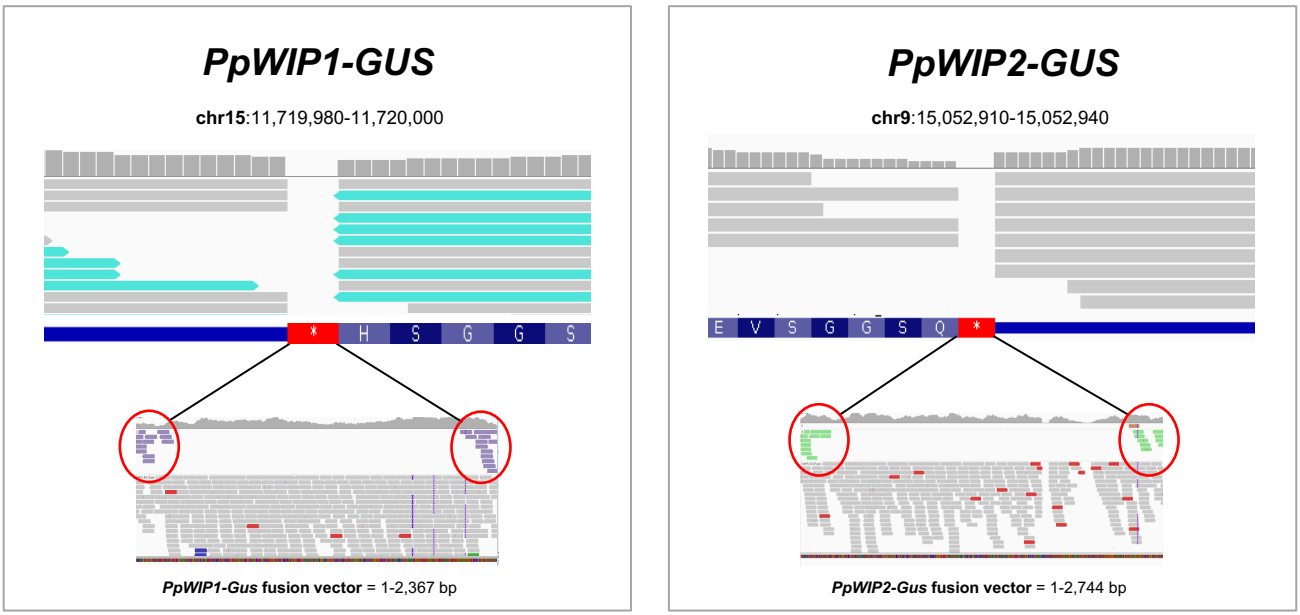

B

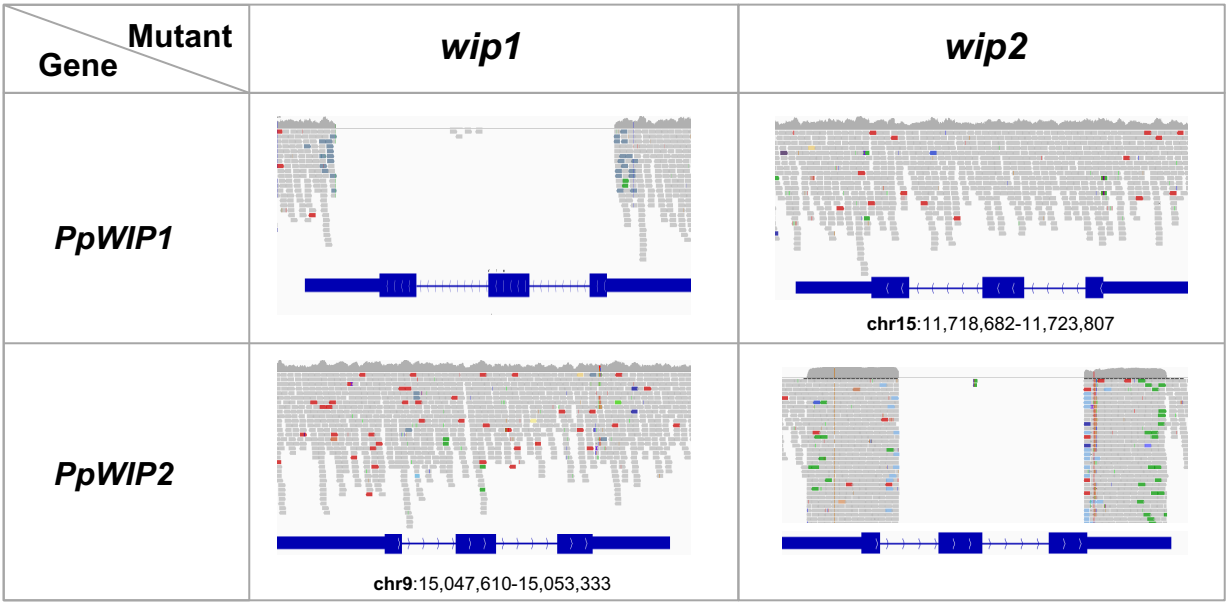

Figure S5. **Genome-wide Illumina sequencing results**. **A)** Reads aligned to the *PpWIP1* and *PpWIP2* loci at the stop codon, corresponding to the insertion site of the β-glucuronidase fusion coding sequence to generate PpWIP1-GUS and PpWIP2-GUS reporter lines. Purple and green reads correspond to paired-end reads in which reads aligns to chromosome 15 and 9 and to *PpWIP1-GUS* and *PpWIP2-GUS* fusion vectors, respectively. **B)** Reads mapped to the *PpWIP1* and *PpWIP2* loci in the *wip1* and *wip2* recombinant mutant lines, respectively. *wip1wip2* mutant shows similar combined reading mapping phenotype than single mutants.

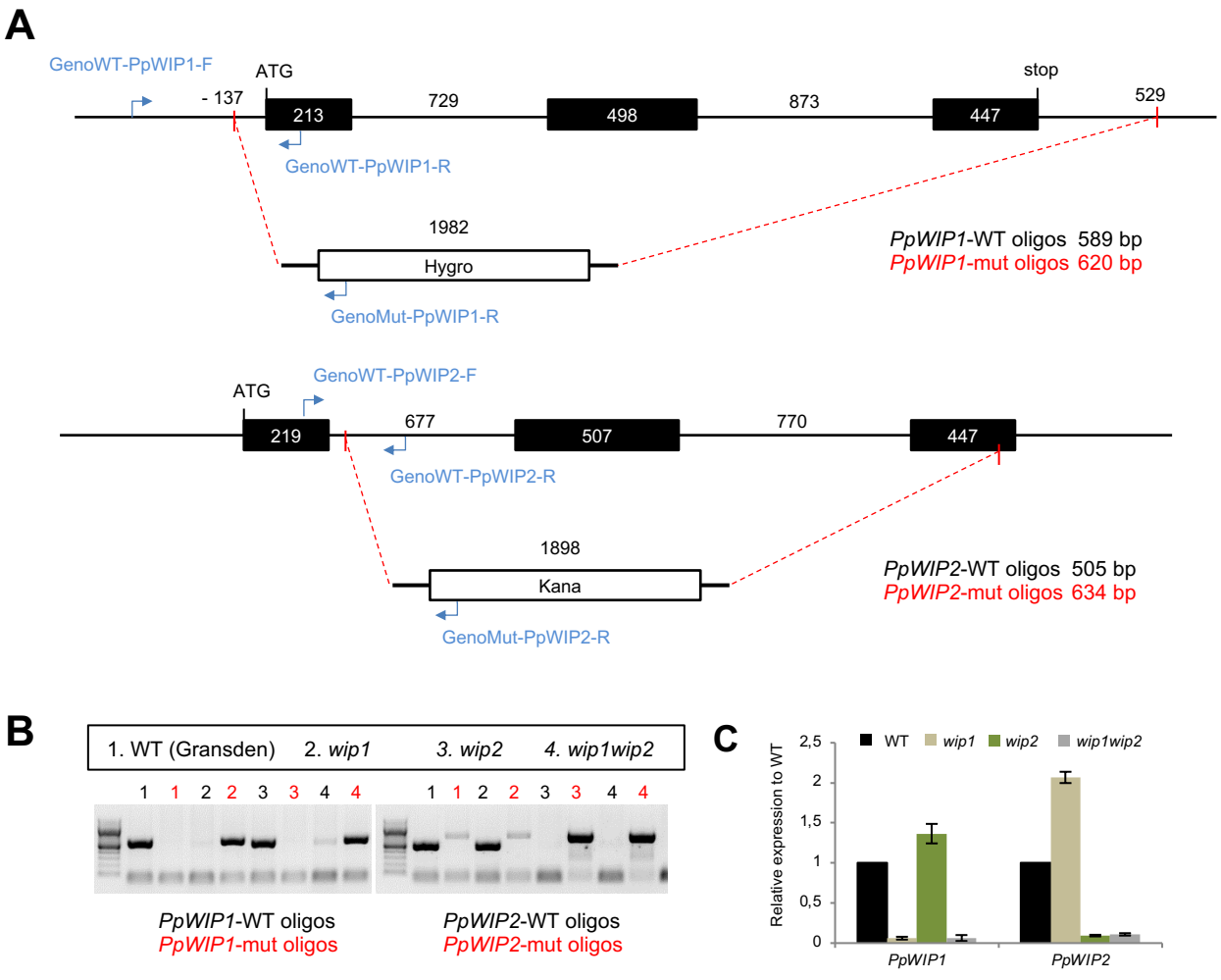

Figure S6. **Targeted gene deletion of *PpWIP1* and *PpWIP2***. A) Schematic representation of the *PpWIP1* and *PpWIP2* loci and corresponding deletions. Arrows indicate the approximate positions of forward and reverse primers used to confirm gene replacement by homologous recombination. B) PCR validation of the gene deletion. C) Relative expression of *PpWIP1* and Pp*WIP2* in WT and *wip* mutants' gametophores, quantified by qRT-PCR (biological replicate *n* = 3, bars = SD).

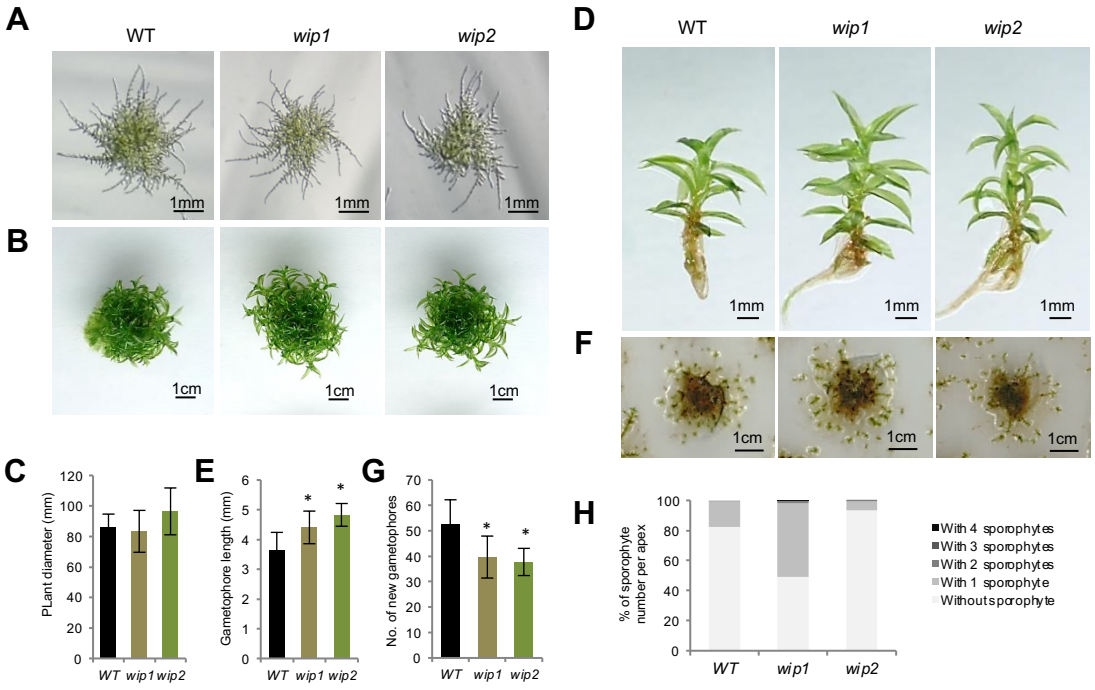

Figure S7. Phenotypic analysis of *wip1* and *wip2* single mutants. A) WT, *wip1*, and *wip2* protonema tissue derived from spores and grown on −AT medium under white light for 11 days. B) Three-week-old WT, *wip1*, and *wip2* plants grown on +AT medium. C) Plant size at 3 weeks (n = 15; bars = SD). D) Gametophores formed from 3-week-old WT, *wip1*, and *wip2* plants grown on +AT medium. E) Length of WT, *wip1* and *wip2* gametophores formed from the 3-week-old plants grown on the +AT medium (*n* = 20; bars = SD; Student's t test *p<0.01). F) Two-month-old WT, *wip1*, and *wip2* plants grown on −AT medium. G) Number of newly formed gametophores per plant after 2 months (*n* = 13; bars = SD; Student's t test *p<0.01). H) Proportion of apices bearing zero, one, or multiple sporophytes in WT, *wip1*, and *wip2* mutants. Two hundred apexes were dissected per genotype from the plants grown under induced condition for 2 months.

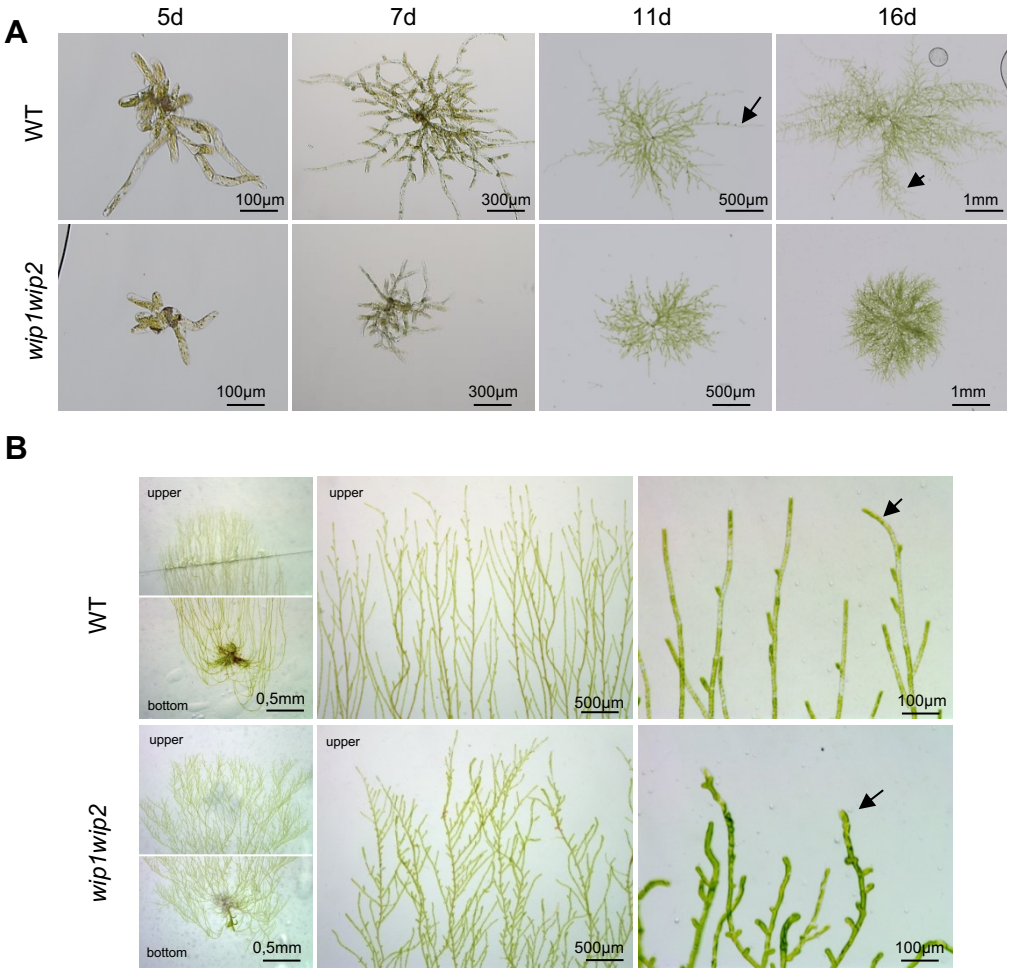

Figure S8. Protonema development in WT and *wip1wip2* double mutant. A) WT and *wip1wip2* protonema tissue derived from spores and grown on −AT medium with cellophane for 16 days. Compared with WT, *wip1wip2* mutants exhibit fewer caulonema or caulonema-like cells (arrows indicate caulonema filaments). B) WT and *wip1wip2* protonema grown under unilateral continuous light for 7 weeks. Pictures of the upper and bottom parts of the colonies are shown. *wip1wip2* protonema is highly branched, and apical cells are predominantly chloronema or caulonema-like. Black arrows mark apical cells in each genotype.

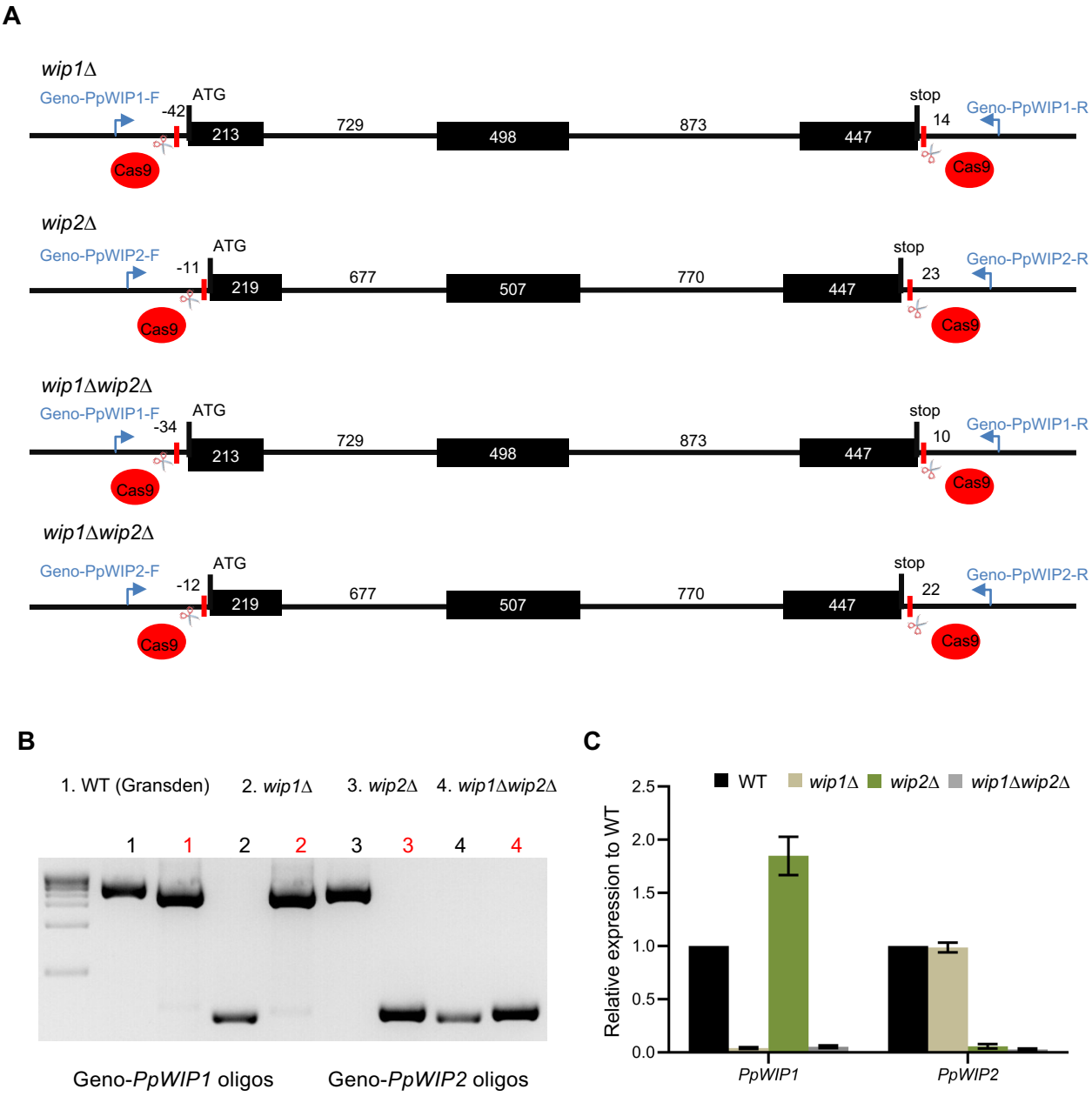

Figure S9. **CRISPR-*Cas9* gene editing of *PpWIP1 and PpWIP2***. A) Scheme of *PpWIP1* and *PpWIP2* loci and the deletions. Arrows represent approximate positions targeted by the forward and reverse primers to determine the transgene. B) PCR validation of the gene deletion. C) Relative expression of *PpWIP1* and *PpWIP2* in WT and *wip*Δ mutants' gametophores, quantified by qRT-PCR (biological replicate *n* = 3, bars = SD).

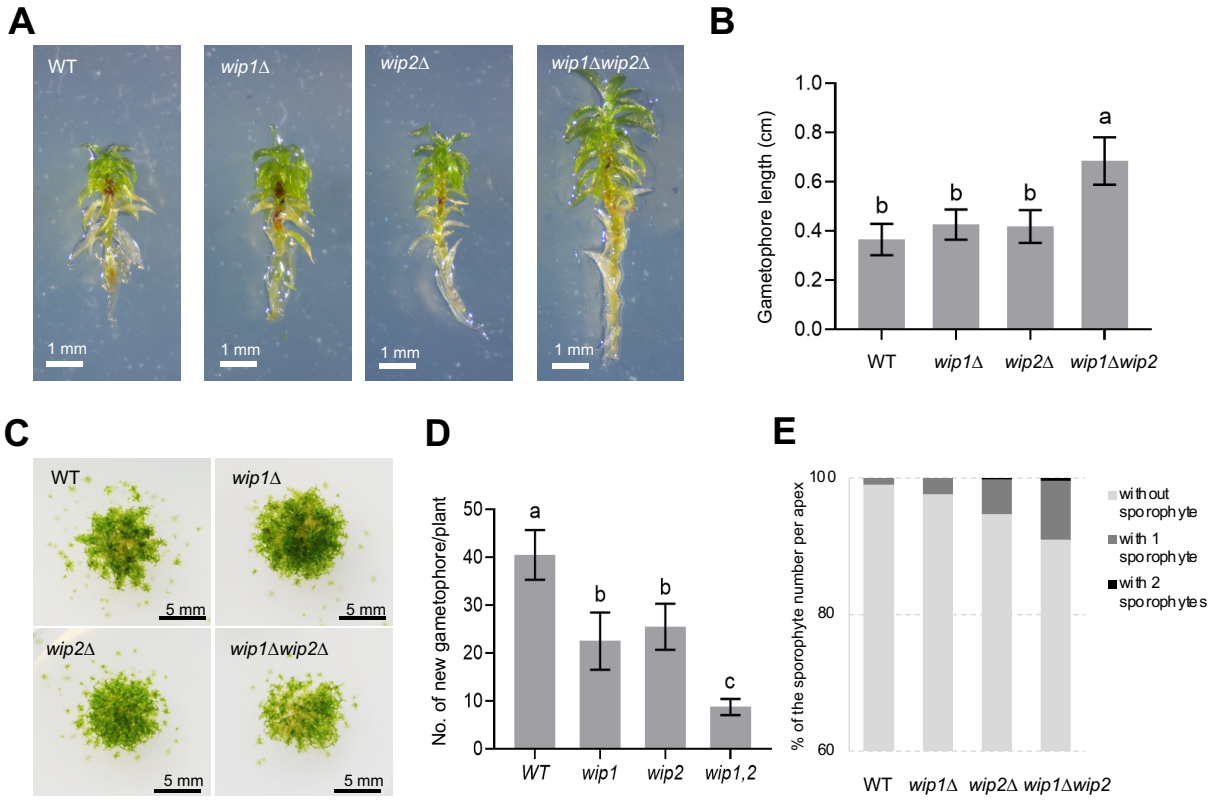

Figure S10. Phenotypes of CRISPR–Cas9–edited *wip*Δ mutants. A) Gametophores of WT, *wip1*Δ, *wip2*Δ, and *wip1*Δ*wip2*Δ derived from 3-week-old plants grown on +AT medium. B) Gametophore length in WT and CRISPR mutant lines after 3 weeks on +AT medium (n = 20; bars = SD; Student's *t* test, **p* < 0.01). C) Two-month-old WT, *wip1*Δ, *wip2*Δ, and *wip1*Δ*wip2*Δ plants grown on −AT medium. D) Number of newly formed gametophores per plant after 2 months (n = 13; bars = SD; Student's *t* test, **p* < 0.01). E) Proportion of apices bearing zero, one, or two sporophytes in WT and CRISPR mutant lines. More than 400 apices were analyzed per genotype from plants grown under sporulation conditions for 3 months (y-axis starts at 60% to enhance visualization of genotype-specific differences). Sporulation assays were performed twice, with >450 gametophores scored per genotype in each experiment.

A

	Reads	Unique_gene_reads	% of mapped reads	Normalised counts
WT-1	25650000	20545912	80.10	19998373.4
WT-2	28060000	21277583	75.83	19593691
wip1-1	28880000	23388372	80.98	20768188.1
wip1-2	23700000	18778292	79.23	20478737.4
wip2-1	19400000	15479955	79.79	20139665.3
wip2-2	21090000	16955140	80.39	19811953.7
wip1wip2-1	32560000	26198571	80.46	19657991
wip1wip2-2	25340000	20513218	80.95	19708033.9

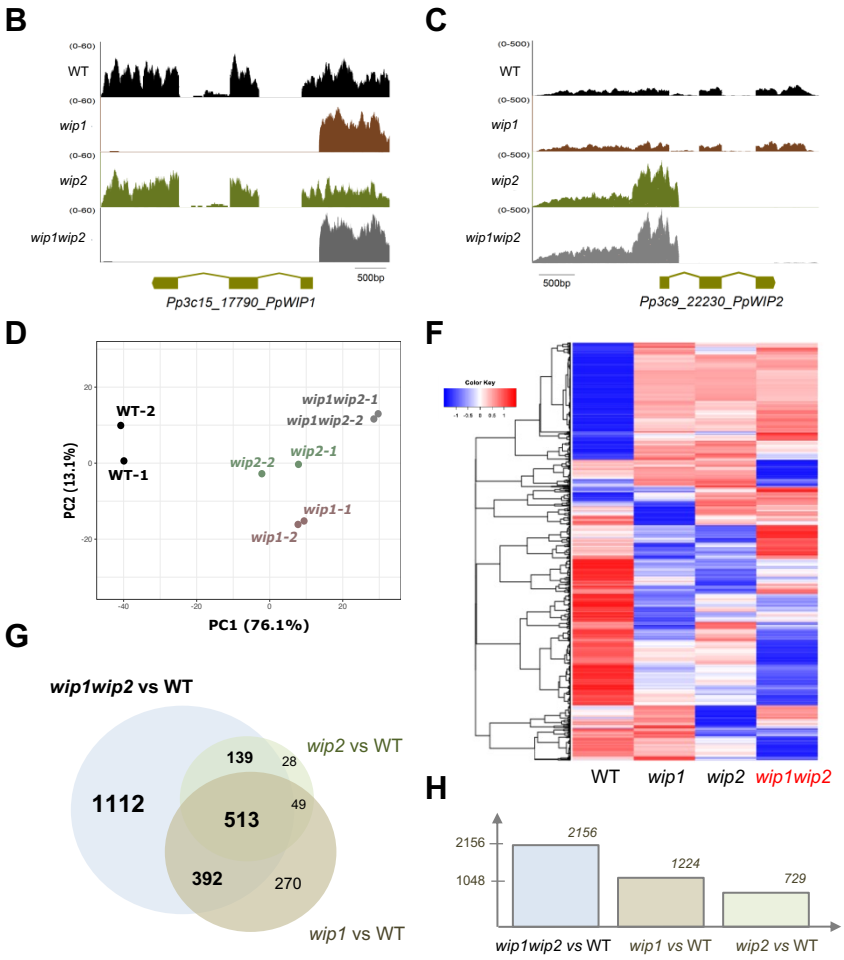

Figure S11. RNA-seq analysis of the transcriptome in WT and *wip* protonema. A) Number of reads obtained in the protonema RNA-seq analysis per sample. B-C) Screen shot of the reads mapped to the (A) Pp*WIP1* and (B) Pp*WIP2* loci in WT, *wip1*, *wip2* and *wip1wip2* mutants. C) PCA analysis showing the different expression profiles among the genotypes and the reproducibility of the two replicates per genotype. D) Hierarchical clustering of the DEGs in *wip1*, *wip2*, and *wip1wip2* (2504 DEGs) mutants versus the WT respectively. E) Venn diagram representing the number of DEGs up- and down-regulated in WT, *wip1*, *wip2*, and *wip1wip2* mutants. F) Histogram showing the number of DEGs up- and down-regulated in WT, *wip1*, *wip2*, and *wip1wip2* mutants.

A

wip1wip2 vs WT		Clusters	
		0-1	4
DEGs	**Genes**	**chloronema**	**caulonema**
up	634	**5.0**	1.4
down	1522	0.8	**2.6**

B

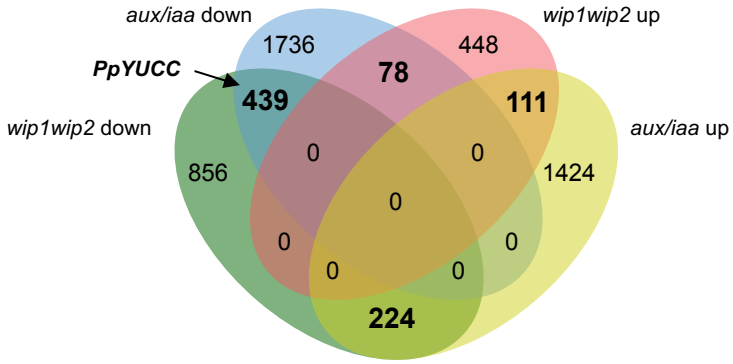

C

Condition	Gene ID	Name	log2FC	padj
WT vs WT+IAA	Pp1s203_59V6	*PpWIP2*	1,36	1,43E-25
WT vs *aux/iaa*	Pp1s203_59V6	*PpWIP2*	2,11	1,07E-63
	Pp1s359_44V6	*PpWIP1*	-0,68	2,58E-12
WT+IAA vs *aux/iaa*+IAA	Pp1s203_59V6	*PpWIP2*	0,70	1,46E-08
	Pp1s359_44V6	*PpWIP1*	-0,96	1,98E-23

Figure S12. Comparison between RNA-seq from *wip1wip2* mutants and other published data. A) Enrichment analysis to compare DEGs genes (up and down) in wip1wip2 mutants to genes associated to choloronema or caulonema (in %), based on single cell data described by Chen *et al.* (2024). B) Venn diagram to compare DEGs up- and down-regulated on protonema of *wip1wip2* and *aux/iaa* mutants related to WT (data described by Lavy *et al.* 2016). C) Expression of *PpWIP1* and *PpWIP2* in the different experiment performed by Lavy *et al.* (2016).

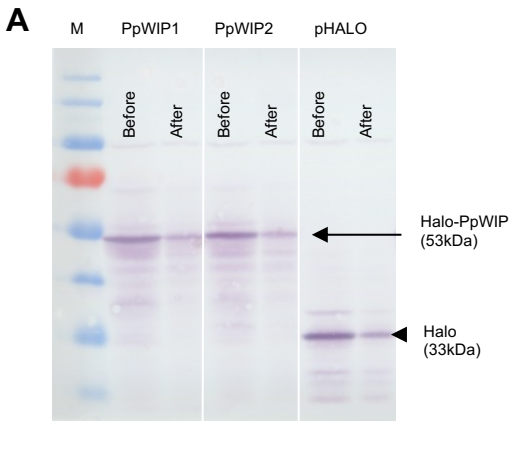

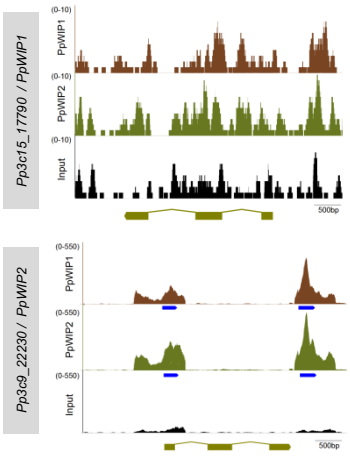

C

Protein	Peaks position	Name	P-value	# Target Sequences with Motif	% Targets Sequences with Motif	# Background Sequences with Motif	% Background Sequences with Motif
PpWIP1-cterm	All peaks	**WIP5** (C2H2)/colamp-DAP-Seq	1e-3753	8415	58.3%	3936	12.2%
		AT1G19040 (NAC)/col-DAP-Seq	1e-1338	3296	22.8%	1394	4.3%
		TCP3 (TCP)/colamp-DAP-Seq	1e-1287	3488	24.1%	1642	5.1%
	Promotors (-3kb)	**WIP5** (C2H2)/colamp-DAP-Seq	1e-734	1580	56.0%	5086	11.1%
		NGA4 (ABI3VP1)/col-DAP-Seq	1e-63	956	33.9%	9299	20.2%
		WRKY46 (WRKY)/colamp-DAP-Seq	1e-38	171	6.1%	861	1.8%
PpWIP2-cterm	All peaks	**WIP5** (C2H2)/colamp-DAP-Seq	1e-1436	3458	55.9%	4725	12.5%
		WRKY27 (WRKY)/colamp-DAP-Seq	1e-1007	3272	52.9%	5841	15.5%
		WRKY15 (WRKY)/col-DAP-Seq	1e-924	3261	52.7%	6222	16.5%
	Promotors (-3kb)	**WIP5** (C2H2)/colamp-DAP-Seq	1e-270	625	51.3%	4916	10.7%
		WRKY46 (WRKY)/colamp-DAP-Seq	1e-26	92	7.5%	913	1.9%
		AT1G19040 (NAC)/col-DAP-Seq	1e-22	107	8.7%	1324	2.8%

Figure S13. DAP-seq analysis of the PpWIP1 and PpWIP2 binding motifs. A) Western blot to show the expression of the fusion proteins (C-terminal of PpWIP1 and PpWIP2). Anti-HaloTag monoclonal antibody was used to label the empty Halo, Halo-PpWIP1 and Halo-PpWIP2 proteins. The expression reaction (before) and the supernatant after the binding (after) were loaded for each condition (two independent replicates were included). B) Detected Halo-PpWIP1 and PpWIP2 binding peaks mapped to the *PpWIP1* and *PpWIP2* loci, compared to control input (*pHALO*). C) Representative known motifs identified on the bound peaks. Similar motifs are detected only in the peaks located in the promoter regions of the targeted genes (-3kb from TSS).

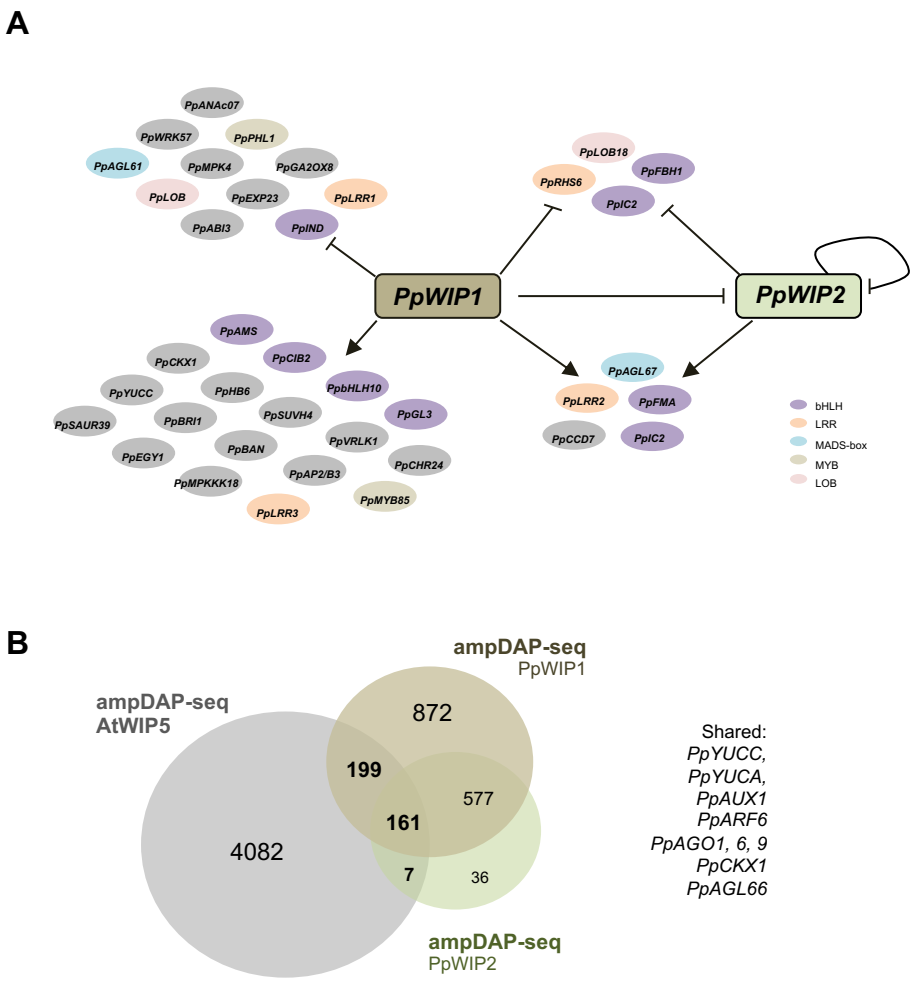

Figure S14. DAP-seq analysis of the PpWIP1 and PpWIP2 binding motifs. A) Putative targeted gene networks of PpWIP1 and PpWIP2, the overlap from the DAP-seq and the RNA-seq (in protonema) data. Lines indicate the induction (with arrows) or repression (with block lines), based on the RNA-seq expression profiles. Targeted genes were classified by the family (different colors). B) Venn diagram comparing bound genes identified by ampDAP-seq for AtWIP5 (O'Malley *et al*. 2016) (36) and for PpWIP1 and PpWIP2 (this study). Several homologue genes involved in auxin biosynthesis (*YUCCA*) or signaling (*AUX1*) were found as targeted by all WIPs.

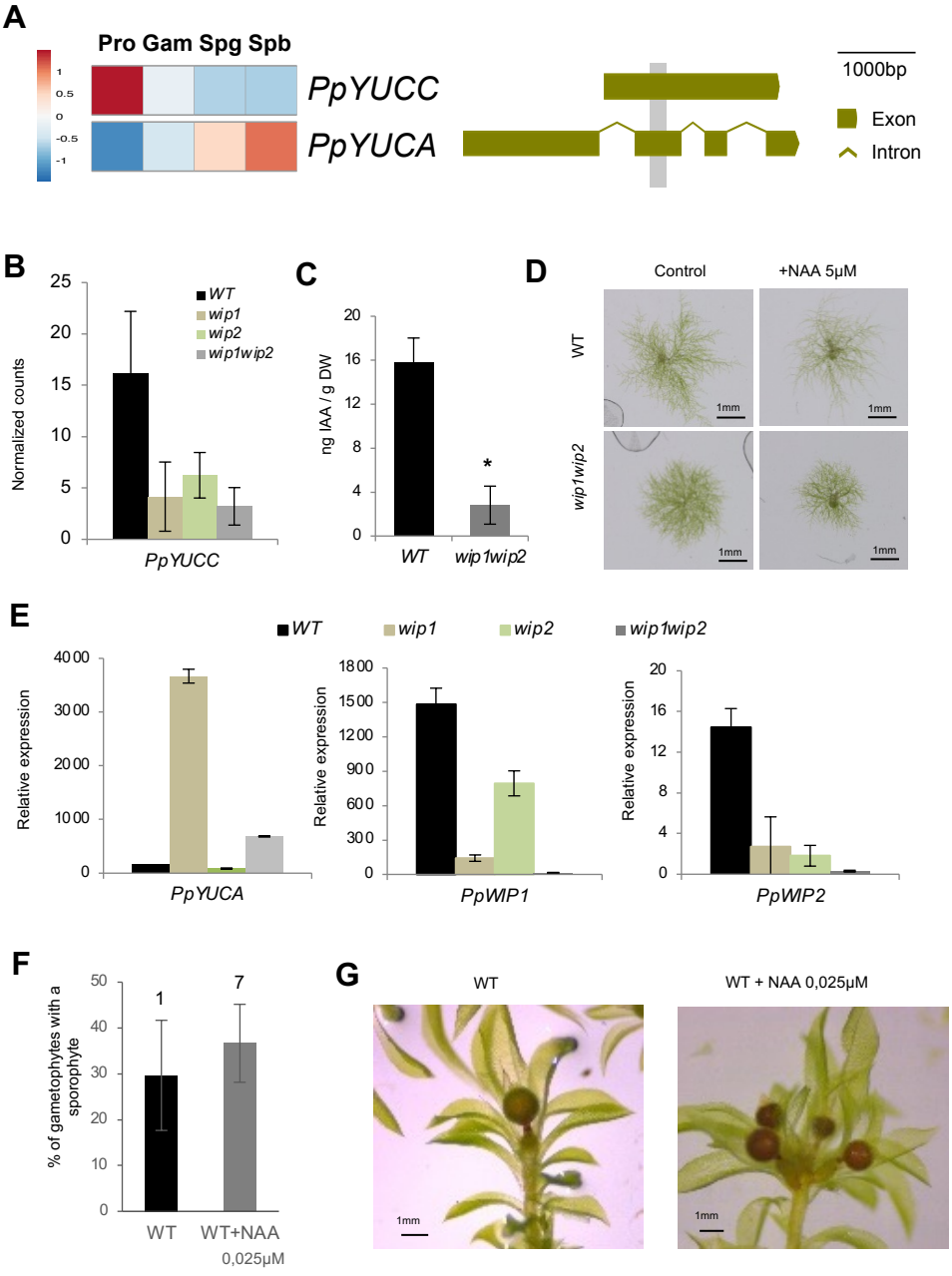

Figure S15. PpWIPs transcriptionally regulate *YUCCA* gene expression. A) Relative gene expression of *PpYUCC* (*Pp3c1_11500*) and *PpYUCA* (*Pp3c3_18590*) in different tissues (data extracted from Perroud *et al*. 2018) (43). *PpYUCC* is mainly expressed in protonema (Pro) and *PpYUCA* in sporophytes (Gam = gametophyte, Spg = green sporophyte, Spb = brown sporophyte). Scheme of the *PpYUCC* and *PpYUCA* loci and location of the peak found in ampDAP-seq of PpWIP1/2 (on gray). B) Expression of *PpYUCC* in protonema of WT, *wip1*, *wip2* and double *wip1wip2* mutants. C) Quantification of the endogenous IAA level by LC-MSMS in WT and *wip1wip2* protonema (n = 3, bars = DS; Student's t test *p<0.001). D) Phenotype of protonema tissue (11 days after sowing) of WT and *wip1,2* mutants treated or not with 5µM NAA, showing not complementation of the mutant phenotype. E) Expression of *PpYUCA, PpWIP1 and PPWIP2* in gametophyte apexes of WT, *wip1*, *wip2* and *wip1wip2* mutants after 30 days sporulation conditions (15°C). F) Percentage of gametophyte apices bearing a single sporophyte in WT plants with or without NAA treatment (0.025 µM). For each condition, three biological replicates were performed, and 100 gametophytes were dissected per replicate. The number of apices bearing more than one sporophytes (from two to four) is indicated in the histogram. G) Pictures of sporophytes dissected in one replicate, showing single and polysety phenotype in WT gametophytes.

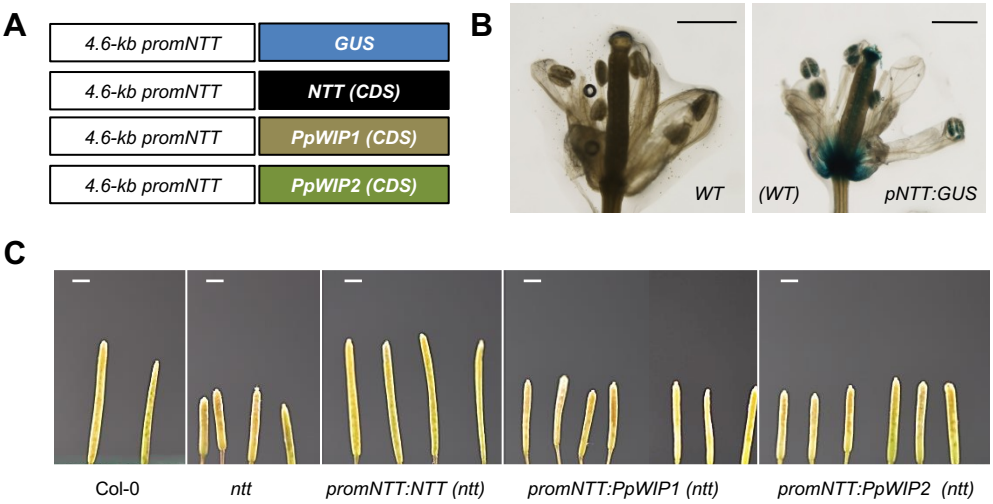

Figure S16. Targeted Pp*WIPs* expression in *ntt* mutants. A) A 4.6-kb At*WIP2/NTT* promotor (*promNTT*) was used to drive expression of *NTT*, Pp*WIP1* and Pp*WIP2* expression in transmitting tracts. B) Gus staining of *promNTT:GUS* in WT flowers. C) Overview of siliques from WT (col-0), *ntt* and *ntt* complemented with *promNTT:NTT*, *promNTT:PpWIP1* and *promNTT:PpWIP2*. Scale bar 1 mm.

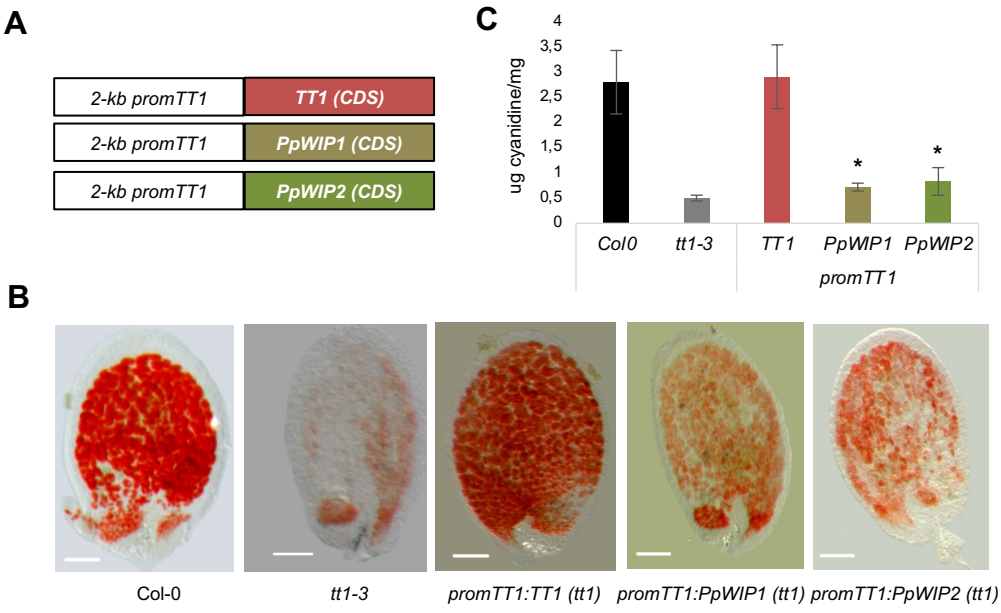

Figure S17. Targeted Pp*WIPs* expression in *tt1* mutants. A) A 2kb At*WIP1/TT1* promotor (*promTT1*) was used to drive expression of *TT1*, Pp*WIP1* and Pp*WIP2* expression in transparent testa *tt1-3* mutants. B) Vanillin staining of *Col-0*, *tt1-3* mutant and *tt1-3* lines complemented with *promTT1:TT1*, *promTT1:PpWIP1* and *promTT1:PpWIP2.* Scale bar= 20 µm. C) Quantification of pro-anthocyanidins (PA) in Col-0, *tt1* and and transgenic immature seeds.